이학박사학위논문

새로운 자가포식작용 조절 단백질의 동정과 그 신호전달체계에 관한 연구

A study on the isolation and signaling of new autophagy regulators

2015년 8월

서울대학교 대학원

유전공학 협동과정

안 혜 현

새로운 자가포식작용 조절 단백질의 동정과 그 신호전달체계에 관한 연구

A study on the isolation and signaling of new autophagy regulators

지도교수 정 용 근

이 논문을 이학박사 학위논문으로 제출함
2015년 6월

서울대학교 대학원
유전공학 협동과정
안 혜 현

안혜현의 이학박사 학위논문을 인준함
2015년 6월

위 원 장 _____(인)
부 위 원 장 _____(인)
위 원 _____(인)
위 원 _____(인)
위 원 _____(인)

A study on the isolation and signaling of new autophagy regulators

A dissertation submitted in partial
Fulfillment of the requirement
for the degree of

DOCTOR OF PHILOSOPHY

to the Faculty of
Interdisciplinary Graduate Program
in Genetic Engineering
at
Seoul National University
by

Hye-Hyun Ahn

Date Approved:
June, 2015

_____

_____

_____

_____

_____

ABSTRACT

A study on the isolation and signaling of new autophagy regulators

Hye-Hyun Ahn

Interdisciplinary Graduate Program

in Genetic Engineering

The Graduate School

Seoul National University

Autophagy is a cellular degradation system for maintaining cellular homeostasis under various stress signals such as nutrient deprivation, hypoxic condition, or endoplasmic reticulum stress. To overcome the stress conditions, cells utilize autophagy-specific proteins to generate double-membrane vesicle called autophagosome to sequester cytosolic components and subcellular organelles fusing with lysosome. However, the precise roles of ATGs and

their regulatory mechanisms are still unknown. To identify novel regulators of autophagy, I employed cell-based functional screening assays using bimolecular fluorescence complementation (BiFC) method.

I found an interaction between ULK1 and ATG9 in mammalian cells and utilized the interaction to identify novel regulators of autophagy upstream of ULK1, an initiation step. I established a cell-based screening assay employing N-terminal Venus-tagged ULK1 and C-terminal Venus-tagged ATG9 BiFC. By performing gain-of-function screening, I identified G6PT as an autophagy activator. G6PT enhanced the interaction between N-terminal Venus (VN)-tagged ULK1 and C-terminal Venus (VC)-tagged ATG9, and increased autophagic flux independent of its transport activity. G6PT negatively regulated mTORC1 activity, demonstrating that G6PT functions upstream of mTORC1 in stimulating autophagy

Also, ATG7-VN/VCn-ATG12 BiFC assay was employed to isolate autophagy modulators which regulate ATG7, an E1-like activating enzyme for ATG12. Utilizing the assay, ZAK was isolated as a potent autophagy activator on elongation step. Expression of ZAK enhanced the fluorescence of ATG7-VN/VCn-ATG12 BiFC assay and increased the interaction between them. ZAK reduced the levels of p62 and ubiquitin conjugates increasing LC3 dot formation. Conversely, malfunction of ZAK expression inhibits autophagy flux. Interestingly, depletion of ZAK blocked amino-acid or serum

starvation-induced autophagy to almost control level. Furthermore, ZAK interacted with ATG7 in mammalian cells. I hypothesize that ZAK is an essential regulator for autophagy activity functioning through its kinase activity and interaction with ATG7.

Keywords: Autophagy, ATGs, G6PT, BiFC, mTORC1, ZAK

***Student Number*:** 2010-30923

CONTENTS

LIST OF FIGURES

ABBREVIATIONS

3MA	3-Methyladenine
ATG	Autophagy-related genes
Baf. A1	Bafilomycin A1
BiFC	Bimolecular Fluorescence Complementation
BSA	Bovine Serum Albumin
DMEM	Dulbecco's Modified Eagle's Medium
EBSS	Earle’s Balanced Salt Solution
ER	Endoplasmic Reticulum
FBS	Fetal Bovine Serum
G6PT	Glucose-6-Phosphate Transporter
GFP	Green Fluorescence Protein
HA	Hemagglutinin
HEK293T	Human Embryonic Kidney 293T

IgG	Immunoglobulin G
IP	Immunoprecipitation
MEF	Mouse Embryonic Fibroblast
PBS	Phosphate Buffered Saline
PFA	Paraformaldehyde
PMSF	Phenylmethylsulfonyl fluoride
PVDF	Polyvinylidene fluoride
RIPA	Radio-Immunoprecipitation Assay
RPMI-1650	Roswell Park Memorial Institute medium
RT-PCR	Reverse Transcription-Polymerase Chain Reaction
SDS-PAGE	Sodium Dodecyl Sulfate-Poly Acrylamide Gel Electrophoresis
shRNA	short-hairpin RNA
ULK1	Specific Pathogen Free
VC	C-terminal fragment of Venus
VN	N-terminal fragment of Venus

CHAPTER I

Identification of glucose-6-phosphate transporter as a key regulator functioning at the autophagy initiation step

Abstract

Autophagy is a common cellular catabolic process involving formation of autophagosome for bulk degradation of proteins via lysosomal pathway. Despite the importance of understanding its regulatory mechanism, the initiation step of autophagy is largely unknown. Here, I show that G6PT regulates autophagy through ULK1 and ATG9. I have found protein-protein interaction between ULK1 and ATG9 in mammalian cells and utilized the interaction to identify the novel regulators at the initiation step of autophagy. I have established a cell-based screening assay employing ULK1-VN and ATG9-VC bimolecular fluorescence complementation (BiFC) assay in live cells. By performing gain-of-functional screening using cDNA expression, I isolated G6PT as a potent autophagy activator enhancing the fluorescence of ULK1-VN and ATG9-VC BiFC. Accordingly, ectopic expression of G6PT increased the binding between ULK1-VN and ATG9-VC and autophagy flux, while knockdown of G6PT expression reduced LC3 dot formation and LC3-II conversion. An increase of autophagic flux by G6PT was through the canonical pathway mediated by ATG5 and full-length of G6PT was required for autophagy regulation independently of its transport activity. In addition,

depletion of G6PT caused the activation of mTORC1, resulting in the inhibition of autophagy induced by Rapamycin, amino acid-starvation, or serum-starvation. These data suggest that G6PT stimulates autophagic flux through negative regulation of mTORC1.

Introduction

Macroautophagy, autophagy hereafter, is an intracellular degradation system and is initiated by the formation of a double-membrane vesicle, called an autophagosome, which fuses with lysosomes to degrade cytoplasmic components (Yang and Klionsky, 2010). Unlike the ubiquitin-proteasome cascade which specifically targets its substrates by ubiquitnation, autophagy degrades subcellular organelles such as mitochondria, peroxisomes and large protein aggregates (Hara et al., 2006). Since autophagy contributes to cell growth, adaptation, and differentiation, its malfunction is intimately associated with human diseases including cancer and neurodegenerative diseases (Jiang and Mizushima, 2014; Kesidou et al., 2013; Nixon, 2013). In early stages of tumorigenesis, autophagy prevents tumor formation by removing the damaged organelles and maintaining genome stability (Matsui et al., 2013). However, as the tumor develops, autophagy gives an advantage to cancer cells for survival. In neurodegenerative diseases, such as Alzheimer's disease and Huntington's disease, the impaired fusion of autophagosomes and lysosome and reduced expression of Beclin 1 and ATG7 polymorphism (V471A) were observed in patient's specimens (Kesidou et al.,

2013). Recent study revealed that atg5 overexpressed transgenic mice showed longevity phenotype meaning that autophagy could regulate the ageing process (Pyo et al., 2013).

Autophagy is tightly regulated by nutritional condition to control the cellular metabolic homeostasis. Autophagy is activated under nutrient deprivation to maintain cellular metabolic homeostasis (Russell et al., 2014). Amino acid starvation induces autophagy by inhibiting mTORC1, which is under the modulation of Rag GTPases (Sancak et al., 2010). During nutrient supplemented condition, mTORC1 inhibits autophagy by phosphorylating ULK1 (Jung et al., 2009) and AMBRA, an E3 ligase, to ubiquitinate ULK1 for degradation (Nazio et al., 2013). During glucose starvation, AMPK activates ULK1 and TSC2 or inhibits Raptor to activate autophagy (Inoki et al., 2003; Kim et al., 2011). Not only controlled by nutrient condition, autophagy is also regulated by cellular stresses. ER stress affects starvation-induced autophagy through eIF2α (Kouroku et al., 2007; Talloczy et al., 2002). However, prolonged ER stress impairs autophagy via IRE1 (Lee et al., 2012). During hypoxia, HIF1α increases BNIP3 and BNIP3L (NIX) to initiate autophagy (Bellot et al., 2009), and PERK increases LC3 and ATG5 to control autophagosome formation (Rouschop et al., 2010). In line with the identification of new autophagy signals, elucidation of signal modulators is necessary for a better understanding of the autophagy mechanism.

To date, about 30 autophagy-related genes (ATGs) have been reported to be required for autophagosome biogenesis (Feng et al., 2014). During autophagosome formation, ATG proteins are recruited to isolation membrane, a precursor of autophagosome, and functions to elongation, curvature, and completion of auotphagosome. Once autophagome is completed, most of ATG proteins are detached from autophagosme. ULK1 complex and class III PI3K complex functions at the initiation/nucleation step. Briefly, ULK1 directly initiate autophagy by upstream kinases such as mTORC1 or AMPK. Class III PI3K generates PI3P which is recognized by FYVE domain (Four cysteine-rich proteins: Fab 1 (yeast orthologue of PIKfyve), YOTB, Vac 1 (vesicle transport protein), and EEA1). FYVE domain containing proteins were recruited to autophagosome assembly site (PAS) to elongate. Two different ubiquitin-like conjugation systems have been reported for autophagosome elongation step. ATG12 and LC3 act like ubiquitin to conjugate with ATG5 and phosphatidylethanolamine (PE). Similar to ubiquitin system, ATG12 and LC3 are first activated by ATG7, an E1-like enzyme, then transferred to ATG10 or ATG3, an E2-like enzymes. Finally, ATG12 forms phosphodiester bond with ATG5. ATG5 further interact with ATG16L1 which forms homodimer. ATG12-ATG5-ATG16L1 complex functions as E3 ligase for LC3-PE conjugation. Autophagosome further fuses with lysosomes. Then inner membrane and sequestered contents in

autophagosome were degraded by lysosomal hydrolases and further released to cytosol.

ULK1 is required for the initiation step of autophagy. ULK1, a serine/threonine kinase, forms complexes with FIP200, ATG13, and ATG101 (Ganley et al., 2009; Hosokawa et al., 2009), and the complexes are mainly controlled by mTORC1 (Ganley et al., 2009; Jung et al., 2009) and AMPK (Kim et al., 2011). The kinase activity of ULK1 is required for the recruitment of VPS34 (PI3K) to isolation membrane (Itakura and Mizushima, 2010; Koyama-Honda et al., 2013). Unlike other ATG proteins, ATG9 is the only membrane protein containing six trans-membrane domains. The function of ATG9 supposed to deliver membrane source for autophagosome expansion, because it shuttles between autophagosomes and the *trans* Golgi network during autophagosome biogenesis (Young et al., 2006). The movement of ATG9 is dependent on the activity of the ULK1 with class III PI3K complex. Moreover, like ATG16L1, ATG9 functions to traffic vesicles derived from the plasma membrane (Puri et al., 2014). In yeast, Atg1, an ULK1 homolog, interacts with Atg9 through Atg17, a counterpart of FIP200, and the interaction is increased by autophagy activation (Sekito et al., 2009). A recent study also reported an interaction between Atg1 and Atg9 in *Drosophila* during starvation-induced autophagy (Tang et al., 2013). However, this interaction has not been revealed in higher eukaryotes.

There are numerous analyses to verify protein-protein interaction. Among them, Bimolecularfluorescence complementation assay (BiFC hereafter) is one of the most superior methods to visualize protein-protein interaction in living cells. The BiFC assay is based on the structural complementation between two non-fluorescent N-terminal and C-terminal fragments of a fluorescent protein. The interaction between the fusion proteins facilitates the association between the fragments of the fluorescent protein. Not only for visualize protein interaction, BiFC also has been used for screening method to identify interactor partners or modifiers of known interactor proteins. It also has been implied screening of small molecule modulators, as those modifiers could change the intensity of fluorescence produced by BiFC assay (Kodama and Hu, 2012).

Glucose-6-phosphate transporter (G6PT) is embedded in the ER membrane by 10 transmembrane domains with its both N- and C- termini on the cytoplasmic side of the ER membrane (Pan et al., 2009). It functions to transport cytosolic glucose-6-phosphate (G6P) into the ER lumen during gluconeogenesis or glycogenolysis by complexing with glucose-6-phosphatase (G6Pase)-α (in the liver, kidney, and intestine) or -β (in neutrophils). Translocated G6P by G6PT is hydrolyzed to glucose and phosphate by G6Pase at the ER lumen where the active site of G6Pase faces. Accordingly, deficiency of G6Pase complex cause glycogen storage disease;

cause of G6Pase-α named GSD1a and cause of G6PT named GSD1b leading to the homeostatic imbalance of glucose (Froissart et al., 2011). However, unlike GSD1a, GSD1b patients show typical phenomenon such as neutropenia, neutrophil dysfunction. More than 160 mutations have been revealed as the causes of GSD1b in patients which disrupt transport activity of G6PT.

To identify novel regulators of the initiation step of autophagy, I performed cell-based functional screening using cDNA expression library. I identified G6PT as an autophagy activator and hypothesized that it regulates autophagy both basal and starvation-induced autophagy through mTORC1 independently of its transport activity.

Materials and Methods

DNA Constructs

The cDNA of G6PT was amplified by PCR using synthetic oligonucleotides (forward 5'-CCC AAG CTT GGG ATG GCA GCC CAG GGC TA-3' and reverse 5'- CCC AAG CTT GGG CTC AGC CTT CTT GGA CA-3') and the PCR products were subcloned into *Hin*dIII site of pcDNA3-HA (Invitrogen). Deletion constructs of G6PT were amplified by PCR and subcloned into *Hin*dIII site of pcDNA3-HA (8TM reverse 5'- CCC AAG CTT GGG AAA CAG GGC AAT GGG-3' and 4TM reverse 5'- CCC AAG CTT GGG GAT GAG CAG GAG ACA-3'). The G6PT shRNAs were constructed using forward and reverse synthetic 19-nucleotides (#1, 1243-CGA AAC ATC CGC ACC AAG A-1261, #2, 107-CAT CAT TGG TGG AAG AGA T-125) which were synthesized, annealed, and cloned into *Bgl*II/*Hin*dIII sites of pSuper-neo (OligoEngine). The full cDNA of ATG9 was amplified by PCR using synthesic oligonucleotides (forward 5'-CCC AAG CTT GGG ATG GCG CAG TTT GAC ACT G-3' and reverse 5'-GGG GTA CCC CTA CCT TGT GCA CCT GAG GGG G-3') and the PCR products were subcloned into *Hin*dIII/*Kpn*I site of pEGFP-N1 (clontech).

Cell Culture and DNA Transfection

HEK293T (human embryonic kidney) cells and m5-7 (mouse fibroblast doxycycline-induced atg5) cells were cultured in DMEM (Hyclone) supplemented with 10 % (v/v) fetal bovine serum (FBS) (Hyclone). Hep3B (human hepatocelluarcarcinoma) cells were cultured in RPMI 1640 (Hyclone) supplemented with 10 % FBS (HyClone) at 37°C under an atmosphere of 5 % CO_2. Transfection was carried out using Polyfect reagent (Qiagen) and mtHTT were transfected using Lipofectamine (Invitrogen) according to the manufacturer's instructions.

Cell-based Functional Screening Assay

ULK1 and ATG9 cDNAs were amplified by PCR using synthetic oligonucleotides (pFLAG-ULK1-VN forward 5'-GAA GAT CTT CCG ATG GAG CCG GGC CGC GGC-3' and pFLAG-ULK1-VN reverse 5'- TGC TCT AGA GCA GGC ATA GAC ACC ACT CAG-3', pHA-ATG9-VC forward 5'-CGG GGT ACC CCG ATG GCG CAG TTT GAC AC-3' and pHA-ATG9-VC reverse 5'- CGG GGT ACC CCG TAC CTT GTG CAC CTG AG-3'). The amplified PCR products were subcloned into *Bgl*II/*Xba*I site of pFlag-VN173

and *Kpn*I site of pHA-VC155. HEK293T cells grown in a 96-well plate were co-transfected with pFLAG-ULK1-VN, pHA-ATG9-VC and an individual cDNA in a mammalian expression vector for 24 h. Serum starvation was treated 3 h before cells were observed under fluorescence microscope used as positive control (Olympus).

Site-directed Mutagenesis

G6PT (R28H, G149E, A373D) mutants were generated by a Quickchange Site-Directed Mutagenesis kit (Stratagene) using synthetic oligonucleotides containing mutations in the corresponding positions. All mutants were verified by DNA sequencing analysis. The nucleotide changes in the mutant constructs include: R28H (82-84, CGC → CAC); G149E (445-447, GGA → GAA); A373D (1117-1119, GCC → GAC).

Generation of Stable Cell Lines

Hep3B cells were transfected with pcDNA3-HA, pG6PT-HA, pSuper-neo or pG6PT shRNA for 24 h and grown in the media containing 1 mg/ml G418 sulfate (Invitrogen) for 2 weeks. Then, single clones of stable cells were isolated using the standard selection method and expression level of each

colony was analyzed by western blot analysis.

Antibodies and Western Blot Analysis

Cells were lyzed in RIPA buffer (50 mM Tris-Cl pH 7.5, 50 mM NaCl, 1% Triton X-100, 0.2% SDS, 1mM EDTA, 1 mM PMSF) and incubated in ice for 15 min. Cell lysates were clarified by centrifugation, resolved by SDS-PAGE, and proteins on gels were transferred to polyvinylidenefluoride membrane (Millipore) using a semidry blotter (Bio-Rad). The membrane was blocked with 5 % BSA in TBS-T (10 mM Tris-Cl, pH 8.0, 150 mM NaCl, 0.5% Tween-20) and incubated overnight at 4 °C with primary antibodies. Immunoblots were visualized by enhanced chemiluminescence method. The following antibodies were used for western blot analysis: LC3, ATG5, Beclin1 (Novus), ATG9A (Novus, Cell signaling), pS6K, S6K, pAMPK, AMPK, p4E-BP1, 4E-BP1, pULK1 (Cell signaling), FLAG (Sigma), p62 (Abnova), actin, ULK1, GFP (Santa Cruz Biotechnology), and G6PT (Abcam).

Immunoprecipitation Assay

Cells were lyzed in RIPA buffer (50 mM Tris-Cl pH 7.5, 50 mM NaCl, 1%

Triton X-100, 0.2% SDS, 1 mM EDTA, and 1 mM PMSF). After clarifying by centrifugation, cell lysates were incubated with anti-ULK1 antibody or FLAG (M2) bead (Sigma) for 12 h at 4°C. After adding protein A/G-Bead (Santa Cruz Biotechnology), the mixtures were incubated for additional 6 h at 4°C. The immunocomplexes were washed five times with PBS, solubilized with sample buffer lacking β-mercaptoethanol, and detected by western blotting.

Immunostaining

Cells grown on coverslips were fixed with 4% paraformaldehyde (PFA) for 15 min, rinsed three times with PBS, permeabilized with 0.1% Triton X-100 for 1 min, and blocked with 1% BSA in PBS for 1 h. After incubation with antibody at 4 °C for 12 h, cells were rinsed with PBS three times, and then incubated with FITC-conjugated or TRITC-conjugated secondary antibodies (Jackson Laboratory Inc.) for 1 h. After rinsing three times with PBS, coverslips were incubated with Hoechst 33258 and placed with mounting medium (Sigma). Cells were visualized under an LSM confocal fluorescence microscope (Zeiss).

RT-PCR

Total RNA was purified using Trizol reagent (Ambion) according to the manufacturer's instructions. The following primer sets were used for PCR: *p62*, forward 5′-ATG GCC ATG TCC TAC GTG AAG GAT G-3′ and reverse 5′-AGA GGG CTA AGG GCA GCT GCC ACA C-3′; *β-actin*, forward 5′-GAG CTG CCT GAC GGC CAG G-3′ and reverse 5′-CAT CTG GAA GGT GGA C-3′.

Filter Trap Assay for mutant Huntingtin Aggregates

HEK293T cells were co-transfected with pHTTex120-GFP and either pSuper-neo, G6PT shRNA #1, or G6PT shRNA #2 for 48 h. Cells showing mtHTT aggregates were observed under a fluorescence microscope. The pHTTex120-GFP, which is a fragment of Huntingtin (HTT) exon1 containing expanded polyglutamine (n=120) fused to GFP, was described (Lee et al., 2012). For filter trap assay, HEK293T cells were transfected with pHTTex120-GFP for 24 h, harvested and washed with ice-cold PBS. Then the cells were briefly lyzed by sonication and added 1% SDS. Prepared samples are subjected to a filter trap using a 96-well dot blot apparatus (Bio-Rad Laboratory). The membrane was washed with PBS containing 1% SDS, blocked with 5 % BSA in TBS-T and then analyzed by western blotting using

anti-GFP antibody.

Statistical Analysis

Differences between groups were analyzed using one-way analysis of variance (ANOVA) followed by Tukey's post-hoc test, or Student's *t*-test, as appropriate. Error bars represent S.D. or S.E.M., as indicated. $P < 0.05$ was considered statistically significant.

Results

Interaction between ULK1 and ATG9 in mammalian cells

Based on the previous reports showing that Atg1 interacts with Atg9 in *Drosophila* and yeast (Sekito et al., 2009; Tang et al., 2013), I first examined whether ULK1 interacts with ATG9 in mammalian cells. Data from the immunoprecipitation assay revealed that ATG9-FLAG interacted with HA-ULK1 in the transfected cells (Figure 1A and B). Moreover, I further found that endogenous ATG9 was immunoprecipitated together with endogenous ULK1 (Figure 1C), indicating that ULK1 interacts with ATG9 in mammalian cells as it revealed in other organism. These results led to establish a screening assay to identify autophagy modulators. Since the BiFC assay is a tool to observe protein-protein interactions in living cells, I adopted this method to identify novel proteins that regulate the initiation step of autophagy around ULK1.

Establishment of the ULK1-VN/ATG9-VC BiFC assay to screen for autophagy activators

To establish the BiFC assay, ULK1 was fused to the N-terminus of

the Venus vector (ULK-VN), while ATG9 was fused to the C-terminus of the vector (ATG9-VC) (Figure 2A). In the immunoprecipitation assay, I detected an interaction between ULK1-VN and ATG9-VC, which was apparently increased under serum starvation (Figure 2B). Following co-expression of ULK1-VN and ATG9-VC, I visualized the GFP-positive signal under a fluorescence microscope. Interestingly, various autophagic stimuli, such as rapamycin-treatment (Rapamycin), serum starvation (Serum (-)), and amino acid starvation (EBSS), significantly increased the fluorescence intensity about 60 % in cells expressing ULK1-VN/ATG9-VC, as compared with the control cells (Figure 2C). Together with result from immunoprecipitation assay, I assumed that interaction between ULK1 and ATG9 is regulated by autophagy stimulation. Therefore, adopting BiFC assay using ULK1-VN and ATG9-VC is suitable for screening. To confirm that fluorescence from BiFC assay is due to specific interaction between ULK1 and ATG9 but not a random collision, I further performed competition assay. The appropriate control of BiFC assay is expression of deletion mutants which interaction domains were removed. However, it was impossible to utilize the deletion mutant to confirm the BiFC assay on my system, therefore I performed competition assay instead. The result from competition assay showed that overexpression of the free form of either ATG9 or ULK1 (cold-ATG9 or -ULK1) together with ULK1-VN/ATG9-VC reduced the fluorescence intensity produced by BiFC

(Figure 2D). To eliminate the possibility that overexpression of both ULK1 and ATG9 fully activates autophagy, I performed western blot analysis to detect autophagy. It revealed that serum starvation following ectopic expression of both ULK1-VN and ATG9-VC further increased LC3-II conversion but decreased the levels of p62 and ubiquitin-conjugates, well-known autophagy substrates (Figure 3A and B). These results indicate that the ULK1-VN/ATG9-VC BiFC assay can be used as a tool for studying the interaction between ULK1 and ATG9, and to identify autophagy regulators that modulate this interaction.

Identification of G6PT as an autophagy activator by cell-based functional screening

By utilizing the ULK1-VN/ATG9-VC BiFC assay, I performed functional screening to isolate autophagy activator after transient expression of each 500 cDNAs which encode endoplasmic reticulum or lysosome-resident proteins in mammalian cells. From the primary screening, I isolated 14 putative positive clones which increased the BiFC fluorescence. From the secondary screening by observing LC3-II conversion, I isolated 5 positive clones. Because glucose-6-phosphate transporter (G6PT) was the most potent to increase both the fluorescence and LC3-II conversion among them, I

further characterized G6PT. As predicted, compared to control cells, ectopic expression of G6PT in HEK293T cells increased the intensity of ULK1-VN/ATG9-VC BiFC about 20% (Figure 4A). Further, data from the immunoprecipitation assay confirmed that G6PT overexpression increased the interaction between ULK1-VN and ATG9-VC (Figure 4B and C). Consequently, ULK1-VN/Atg9-VC BiFC assay allowed me to successfully isolate autophagy activators from cDNA expression library, such as G6PT.

Ectopic expression of G6PT increased autophagy flux

To investigate whether G6PT enhance autophagic flux, I ectopically expressed G6PT in HEK293T cells and observed that G6PT increased LC3-II conversion by western blot analysis. Because increment of LC3-II conversion does not fully understand for autophagy activation, further the cells were treated with Bafilomycin A1, a lysosomal inhibitor, to block lysosomal degradation and found that treatment of Bafilomycin A1 further increased LC3-II conversion (Figure 5A). Then I generated Hep3B cells expressing G6PT-HA stably (Figure 5B). Western blot analysis showed that LC3-II conversion was increased in Hep3B/G6PT-HA cells as compared with control cells, and this increment was further enhanced by the treatment with Bafilomycin A1 (Figure 5C). This indicates that the increment of LC3-II

conversion by G6PT overexpression is due to the activation of autophagy, but not inhibition of autophagy flux as I observed in HEK293T cells. Similar results were also observed using the GFP-LC3 puncta formation assay. Increased GFP-LC3 puncta by G6PT overexpression and further enhanced GFP-LC3 puncta formation under Bafilomycin A1 treatment (Figure 5D). Autophagic flux was further assessed with the mCherry-GFP-LC3 assay. Because mCherry is more stable in acidic pH than that acid-labile GFP, mCherry-only signal increases during autophagy activation. The results revealed that Hep3B cells expressing G6PT-HA showed great increment of red LC3 puncta (5-folds) as well as yellow LC3 puncta (2-folds) (Figure 5E and F), indicating that G6PT expression increased the formation of both autophagosomes and autolysosomes. Together, these data indicate that the increases of LC3 puncta formation and LC3-II level by G6PT overexpression are not due to blockage of the fusion of autophagosome with lysosome but are affected by the increase in autophagy flux.

Beclin1 and ATG5-dependent regulation of G6PT-mediated autophagic flux

The depletion of Beclin1, a key component of class III PI3K complex that regulates autophagy at the initiation step, blocked the increase in GFP-

LC3 puncta induced by G6PT expression (Figure 6A). This result indicates that G6PT regulates autophagy at the initiation step, especially upstream of class III PI3K. Therefore it is appropriate for screening assay which propose to isolate autophagy regulator modulating at initiation step. As a recent study reported that alternative macroautophagy can occur independent of ATG5/ATG7 (Nishida et al., 2009), I tested whether this mechanism is involved in G6PT-induced autophagy using conditional *Atg5*-knockout mouse embryo fibroblasts (MEFs) (Hosokawa et al., 2006). Similar to the results obtained from experiments using Hep3B cells, ectopic expression of G6PT increased GFP-LC3 puncta formation in wild-type but not *Atg5*$^{-/-}$ MEFs (Figure 6B). This indicates that G6PT activates autophagy in an ATG5-dependent manner.

Depletion of G6PT caused accumulation of autophagy substrates by inhibiting autophagy activity

Subsequently, I generated stable G6PT knockdown Hep3B cells (Hep3B/G6PT shRNA #1 and #2) to assess the effects of G6PT knockdown on autophagy. Using western blot analysis by anti-G6PT antibody, I detected two bands. Because there are actually five isoforms of G6PT with different sizes and among them, two bands were all reduced by G6PT knockdown, I

believe that those bands are G6PT isoforms. (Figure 7A). In comparison with control cells, Hep3B/G6PT shRNA cells exhibited a reduced basal level of LC3-II and an increased accumulation of autophagy substrates such as ubiquitin-conjugates and p62 (Figure 7B) (Ichimura et al., 2008). Similarly, monitoring the level of endogenous p62 with immunocytochemical analysis revealed the enhanced levels of p62 aggregates in G6PT-knockdown cells (Figure 7C). To identify whether the change of p62 level was not due to alteration of the mRNA level, I assessed RT-PCR to quantify mRNA levels in Hep3B/G6PT shRNA cells and observed no alteration in p62 mRNA level. Thus, accumulation of p62 in Hep3B/G6PT shRNA is due to inhibition of autophagy (Figure 7D). I also measured the aggregation of mutant Huntingtin (mtHTT), an autophagy substrate (Lee et al., 2012), in G6PT knockdown cells. Using the filter trap assay, I found that knockdown of G6PT expression increased the aggregation of GFP-fused mtHTT (Figure 8A and B). Consistent with the stimulatory effects of G6PT expression on autophagy, these results indicate that G6PT is crucial in autophagy activation.

G6PT modulated autophagy independent of its transport activity

Because G6PT functions as a transporter that dispatches cytosolic G6P into the ER lumen, I addressed whether the transport activity of G6PT is

associated with its autophagy activity. Based on a previous report (Chen et al., 2008a), I generated several transport activity-dead mutants of G6PT and tested their effects on autophagy. Like wild-type G6PT, all of the G6PT transport activity-dead mutants increased the levels of LC3-II conversion, GFP-LC3 positive puncta, and the fluorescence intensity in the ULK1-VN/ATG9-VC BiFC assay (Figure 9A-C). Further, treatment with chlorogenic acid (CHA), an inhibitor of G6PT (Chen et al., 2008b), did not inhibit LC3-II conversion and GFP-LC3 puncta formation (Figure 9D and E). Consistently, I further tested whether G6PT transport activity is dispensable for autophagy activation using HT22 cells, non-gluconeogenetic cells. G6PT still increased LC3-II conversion and GFP-LC3 puncta formation in HT22 cells. Moreover, ectopic expression of G6PT increased DFCP1-GFP puncta in HT22 cells (Figure 10A-C). These results indicate that G6PT affects autophagy activity in a transport activity-independent manner.

C-terminus of G6PT might function to regulate autophagy

The transport activity-independent function of G6PT in autophagy stimulation led to define the functional domain responsible for autophagy in G6PT. G6PT is composed of 10 transmembrane domains. Therefore, I deleted several transmembrane domains to generate C-terminal deletion mutants of

G6PT and tested their activities on autophagy (Figure 11A). In comparison with wild-type, G6PT deletion mutants were rapidly degraded in the transfected cells and thus detected only in the presence of MG132, a proteasome inhibitor. G6PT deletion mutants containing the N-terminal 4 or 8 transmembrane domains but lacking the C-terminal transmembrane domains failed to increase GFP-LC3 puncta formation and LC3-II conversion (Figure 11B and C), indicating that the C-terminal region of G6PT may be required for its autophagy activity.

G6PT activated autophagy by inhibiting mTORC1 during amino acid starvation

In addition to its contribution to basal autophagy, I further assessed the role of G6PT in amino acid starvation-induced autophagy. Surprisingly, under amino acid starvation (with EBSS), the formation of both endogenous and ectopic LC3-positive puncta were abolished in Hep3B/G6PT shRNA cells but not in Hep3B control cells (Figure 12A and B). Additionally, LC3-II level was decreased under amino acid starvation in Hep3B/G6PT shRNA cells compare to those of control cells (Fig. 12C). I further observed that subcellular distribution of ATG9-GFP were impaired in Hep3B/G6PT shRNA cells during amino acid starvation (Figure 13A and B). Because mTORC1 is

inactivated by amino acid starvation, I further illustrated that autophagy inhibitory effect in G6PT knockdown stable cells during amino acid starvation-induced autophagy is mediated by mTORC1. Western blot analysis illustrated that G6PT knockdown increased the level of phosphorylated S6 kinase (Thr 389) and 4E-BP1 (Thr 37/46), direct substrates of mTORC1 (Ma and Blenis, 2009), on both nutrient supplemented and amino acid starved condition (Figure 14A). Also, this increment was eliminated by the treatment with Rapamycin, a mTORC1 inhibitor. Moreover, rapamycin treatment restored the level of LC3-II in Hep3B/G6PT shRNA cells (Figure 14B). Simultaneously, ULK1 phosphorylation S638 by mTORC1 was increased by G6PT knockdown but decreased by G6PT overexpression in Hep3B cells (Figure 14C and 15C). These results indicate that G6PT regulates autophagy through the inhibition of mTORC1 both basal and amino acid starvation-induced autophagy.

Down regulation of G6PT inhibits glucose starvation-induced autophagy by activating AMPK

Because G6PT regulates autophagy separately with its transport activity, I assumed that G6PT regulates glucose starvation-induced autophagy besides amino acid starvation-induced autophagy. I observed that under

glucose starvation, G6PT knockdown reduced LC3-II conversion and GFP-LC3 puncta formation. I further identified that the level of phosphorylated AMPK (T172) is reduced in Hep3B stably expressed G6PT shRNA during glucose starvation (Figure 15A and B). On the other hand, the phosphorylation of ULK S555 by AMPKα was increased by G6PT overexpression. Likewise wild-type G6PT, G6PT mutants similarly regulate mTORC1 and AMPKα (Figure 15C). Together, these data indicate that G6PT regulates autophagy through the inhibition of mTORC1 and activation of AMPK during starvation-induced autophagy.

Figure I-1. Interaction between ULK1 and ATG9 in mammalian cells. (A and B) Interaction between ATG9-FLAG and HA-ULK1 in mammalian cells. HEK293T cells were co-transfected with pATG9-FLAG and pHA-ULK1 for 24 h. Cell extracts were subjected to immunoprecipitation (IP) assay with anti-HA antibody (A) or anti-FLAG (M2) antibody (B). The immunoprecipitates and whole cell lysates (WCL) were analyzed by western blot analysis. (C) Endogenous interaction between ULK1 and ATG9. HEK293T cell extracts were subjected to immunoprecipitation assay using anti-ULK1 antibody. Asterisk indicates non-specific signal.

Figure I-1

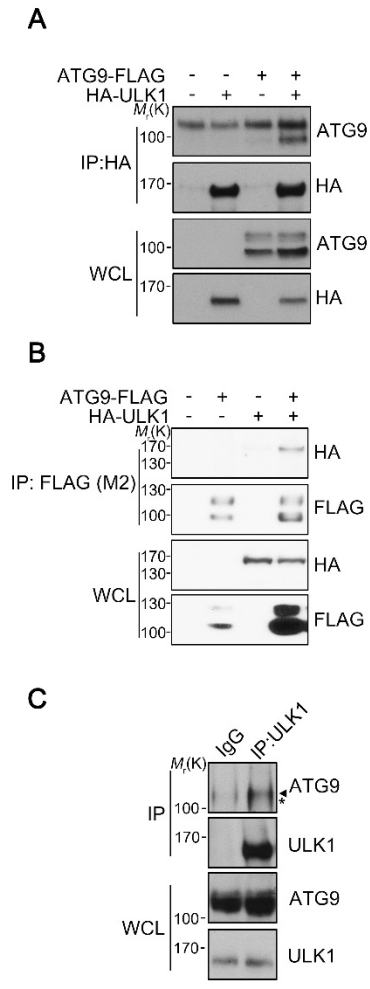
A
ATG9-FLAG - - + +
HA-ULK1 - + - +
M_r(K)
IP:HA
100
170
ATG9
HA
WCL
100
170
ATG9
HA
B
ATG9-FLAG - + - +
HA-ULK1 - - + +
M_r(K)
IP: FLAG (M2)
170
130
HA
130
100
FLAG
WCL
170
130
HA
130
100
FLAG
C
IgG
IP:ULK1
M_r(K)
IP
100
170
ATG9
ULK1
WCL
100
170
ATG9
ULK1

Figure I-2. Establishment of the ULK1-VN/ATG9-VC BiFC assay to screen autophagy activators. (A) Schematic diagram showing the BiFC assay using ULK1 and ATG9 as interacting proteins. A fluorescence protein, VENUS, is split into two parts. The parts containing the N- and C-terminal of VENUS, termed VN and VC, respectively, are fused with ULK1 and ATG9, respectively. Interaction between ULK1 and ATG9 brings VN and VC to a close proximity, generating a fluorescence signal that can be detected under a fluorescence microscope. (B) Increased interaction between FLAG-ULK1-VN and HA-ATG9-VC under serum starvation. HEK293T cells were co-transfected with pHA-ATG9-VC and pFLAG-ULK1-VN for 19 h and then incubated with either serum-supplemented or serum-free medium for an additional 3 h. Cell extracts were immunoprecipitated with anti-FLAG (M2) antibody. (C) Visualization of ULK1-VN/ATG9-VC association in living cells. HEK293T cells were co-transfected with pHA-ATG9-VC and pFLAG-ULK1-VN for 19 h and then incubated with serum-supplemented, Rapamycin-containing (0.1 μg/ml) (Rapamycin), serum-free (Serum (−)), or amino acid-free medium (EBSS) for additional 3 h. Green fluorescence images of the complementation were acquired under a fluorescence microscope (GFP channel). Relative intensity of the BiFC fluorescence was measured using Multi Gauge V3.0 (Fuji film). Bars represent mean values ± S.E.M (n = 100). *** $P < 0.001$. (D) Competition assay showing the specific

interaction between ULK1-VN and ATG9-VC. HEK293T cells were co-transfected with pFLAG-ULK1-VN, pHA-ATG9-VC, and either pATG9 (cold ATG9) or pULK1 (cold ULK1) and cultivated in growth medium for 24 h. GFP signals were observed under a fluorescence microscope and the relative intensity of the BiFC fluorescence was measured. ** $P < 0.01$, *** $P < 0.001$.

Figure I-2

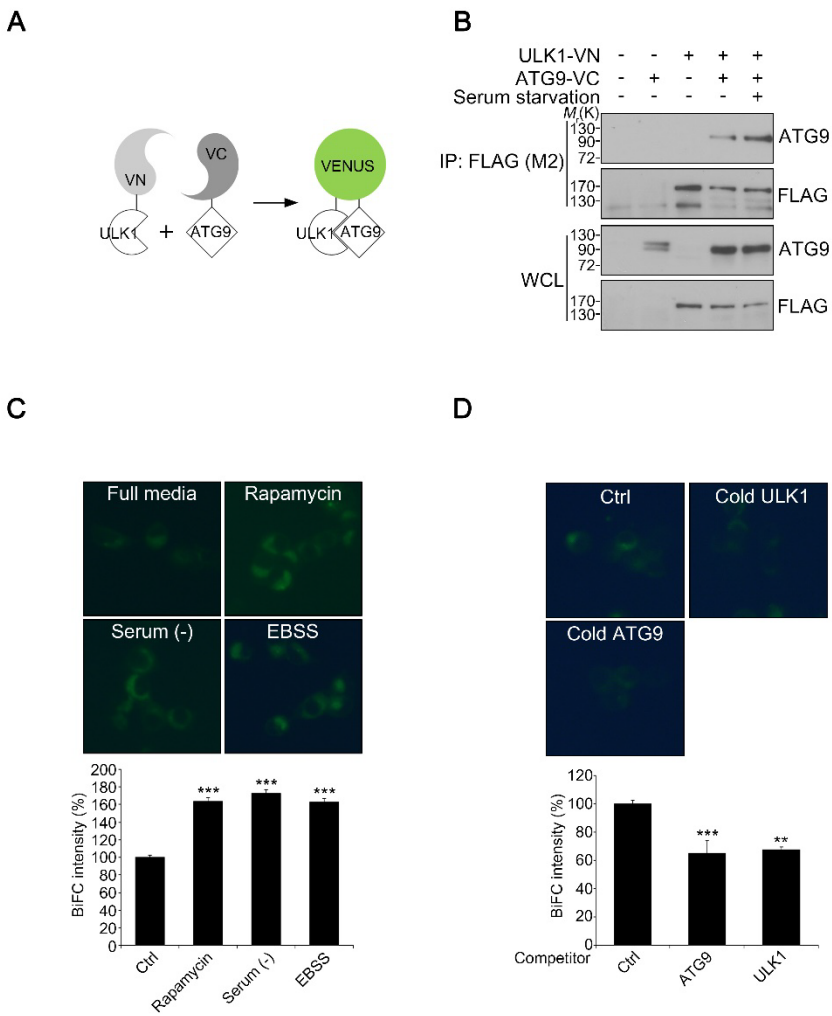
A
VN
VC
VENUS
ULK1
ATG9
ULK1
ATG9
B
ULK1-VN - - + + +
ATG9-VC - + - + +
Serum starvation - - - - +
M.(K)
130
90
72
ATG9
IP: FLAG (M2)
170
130
FLAG
130
90
72
ATG9
WCL
170
130
FLAG
C
Full media
Rapamycin
Serum (-)
EBSS
BiFC intensity (%)
200
180
160
140
120
100
80
60
40
20
0
***
***
***
Ctrl
Rapamycin
Serum (-)
EBSS
D
Ctrl
Cold ULK1
Cold ATG9
BiFC intensity (%)
120
100
80
60
40
20
0
***
**
Competitor
Ctrl
ATG9
ULK1

Figure I-3. Expression of ULK1-VN and ATG9-VC increased autophagy. (A and B) Effects of serum starvation on autophagy in ULK1/ATG9 BiFC assay. HEK293T cells were co-transfected with pHA-ATG9-VC and pFLAG-ULK1-VN for 19 h and then incubated with either complete medium or serum-free medium for additional 3 h. Cell extracts were examined with western blot analysis. Relative intensity of the western blot was measured using ImageJ 1.48v.

Figure I-3

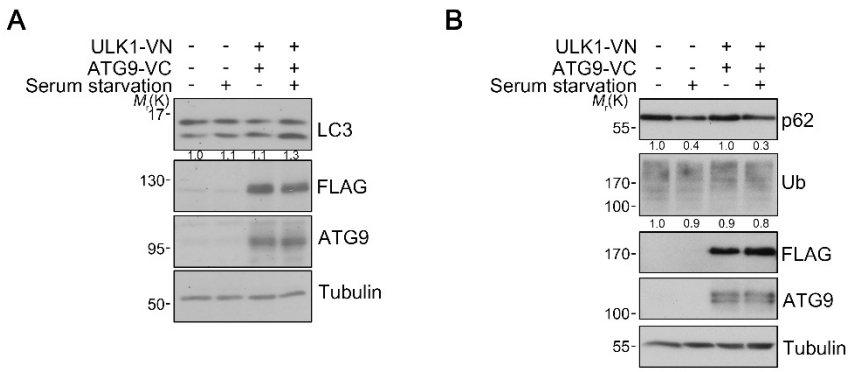
A
ULK1-VN - - + +
ATG9-VC - - + +
Serum starvation - + - +
M_r(K)
17-
LC3
1.0 1.1 1.1 1.3
130-
FLAG
95-
ATG9
50-
Tubulin
B
ULK1-VN - - + +
ATG9-VC - - + +
Serum starvation - + - +
M_r(K)
55-
p62
1.0 0.4 1.0 0.3
170-
100-
Ub
1.0 0.9 0.9 0.8
170-
FLAG
100-
ATG9
55-
Tubulin

Figure I-4. Identification of G6PT as an autophagy activator by cell-based functional screening. (A) Enhanced BiFC signals of ULK1-VN/ATG9-VC by G6PT overexpression. HEK293T cells were co-transfected with pHA-ATG9-VC, pFLAG-ULK1-VN, and either pcDNA3-HA (Ctrl) or pG6PT-HA for 24 h. Green fluorescence images of the complementation were acquired under a fluorescence microscope (GFP channel) (*upper*) and quantified using Multi Gauge V3.0 (Fuji film) (*lower*). * $P < 0.05$. (B) Enhanced binding between ATG9-VC and ULK1-VN by G6PT expression. After transfection with pHA-ATG9-VC, pFLAG-ULK1-VN, and either pcDNA3-HA or pG6PT-HA for 24 h, HEK293T cell extracts were analyzed with immunoprecipitation assay using anti-FLAG (M2) antibody. (C) Enhanced interaction between ATG9-VC and ULK1-VN by G6PT overexpression. HEK293T cells were co-transfected with pHA-ATG9-VC, pFLAG-ULK1-VN, and either pCMV-3xFLAG or pFLAG-G6PT for 24 h. Cell extracts were subjected to immunoprecipitation (IP) assay with anti-HA antibody. The immunoprecipitates and whole cell lysates (WCL) were analyzed by western blot analysis.

Figure I-4

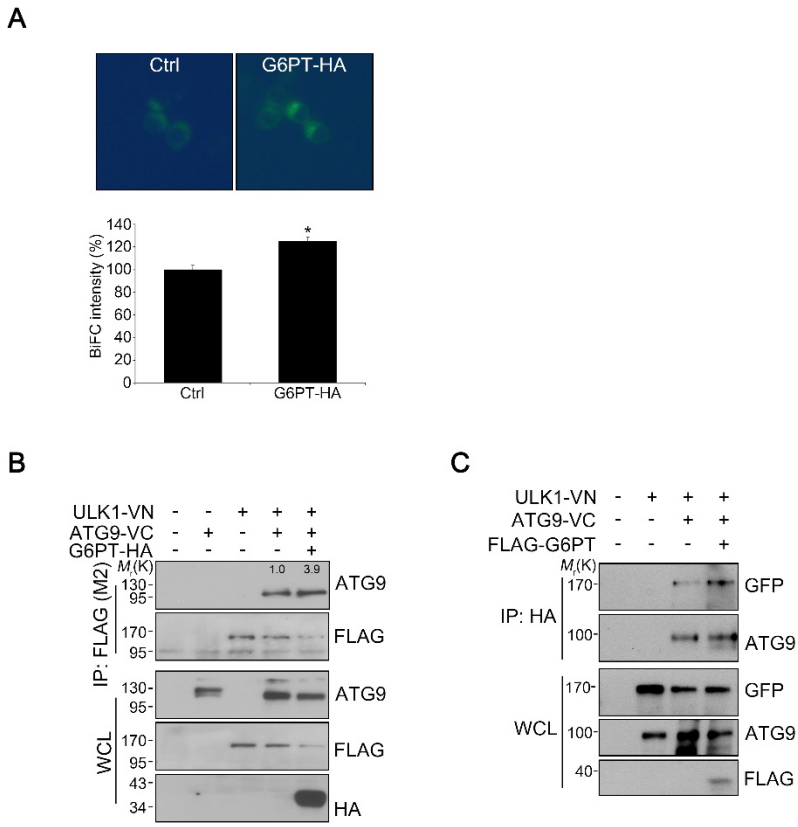
A
Ctrl
G6PT-HA
BiFC intensity (%)
140
120
100
80
60
40
20
0
*
Ctrl
G6PT-HA
B
ULK1-VN - - + + +
ATG9-VC - + - + +
G6PT-HA - - - - +
M1(K)
IP: FLAG (M2)
WCL
130
95
170
95
130
95
170
95
43
34
1.0
3.9
ATG9
FLAG
ATG9
FLAG
HA
C
ULK1-VN - + + +
ATG9-VC - - + +
FLAG-G6PT - - - +
M1(K)
IP: HA
WCL
170
100
170
100
40
GFP
ATG9
GFP
ATG9
FLAG

Figure I-5. Ectopic expression of G6PT increased autophagy. (A) Increased LC3-II conversion by G6PT overexpression. HEK293T cells were transfected with pcDNA3-HA or pG6PT-HA for 24 h and then left untreated or incubated with 10 nM Bafilomycin A1 (Baf. A1) for 2 h before harvested. Cell extracts were analyzed with western blot analysis. (B) Generation of Hep3B/G6PT-HA stable cells. Hep3B cells were transfected with pcDNA3-HA (Ctrl) or pG6PT-HA for 24 h, and then selected with G418 (1 mg/ml) for 2 weeks. G6PT-HA expression was detected by western blot analysis. (C and D) Increase of autophagy activity by G6PT expression. Hep3B/Ctrl and Hep3B/G6PT-HA cells were either untreated or exposed to 10 nM Bafilomycin A1 (Baf. A1) for 2 h and cell extracts were subjected to western blot analysis (C). Hep3B/Ctrl and Hep3B/G6PT-HA cells were transfected with pEGFP-LC3 for 24 h in the presence or absence of 10 nM Baf. A1 Cells showing GFP-LC3 puncta (> 5) were counted under a fluorescence microscope (D). ** $P < 0.01$, *** $P < 0.001$. (E and F) Regulation of autophagic flux by G6PT expression. Hep3B/Ctrl and Hep3B/G6PT-HA cells grown on coverslips were transfected with pmCherry-GFP-LC3 for 24 h. After fixing the cells with 4% paraformaldehyde, green (*upper*) and red (*middle*) fluorescence images were acquired under a confocal microscope (E). The number of LC3 puncta showing GFP^+/RFP^+ or GFP^-/RFP^+ were counted and represented with bars (mean values ± S.E.M., $n = 15$). ** $P < 0.01$, ***

$P < 0.001$ (F).

Figure I-5

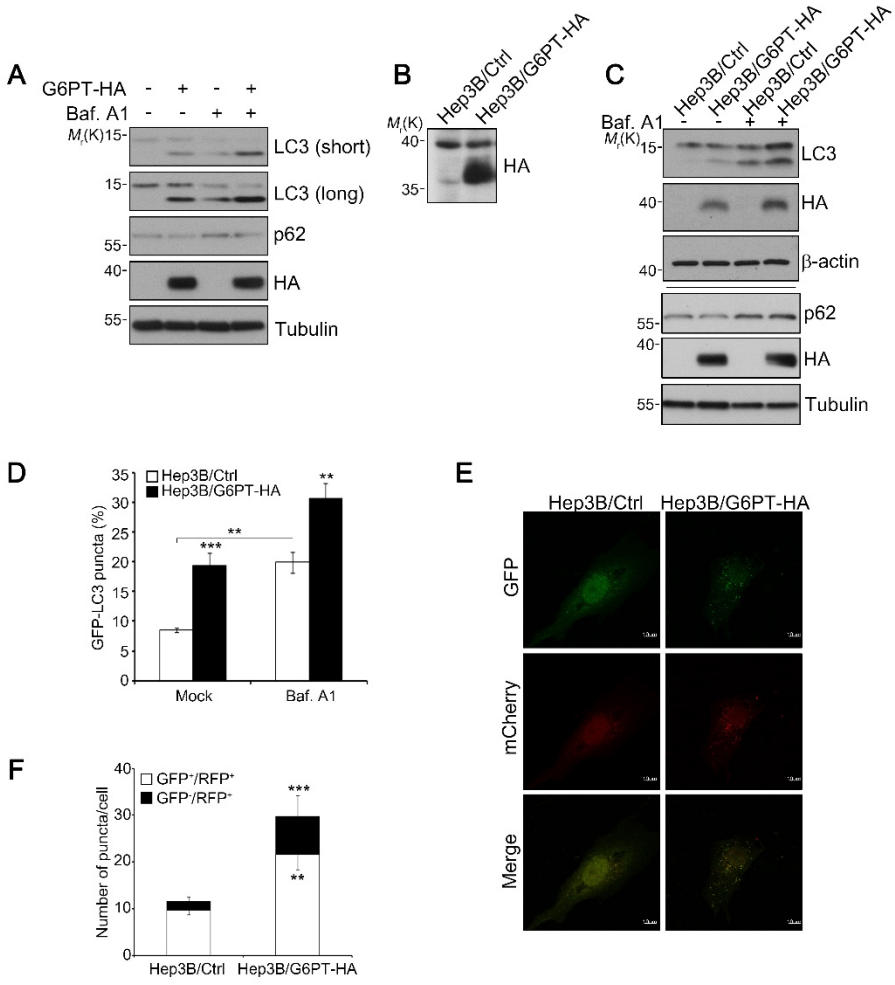
A
G6PT-HA - + - +
Baf. A1 - - + +
M_r(K)
15
LC3 (short)
15
LC3 (long)
55
p62
40
HA
55
Tubulin
B
Hep3B/Ctrl
Hep3B/G6PT-HA
M_r(K)
40
35
HA
C
Hep3B/Ctrl
Hep3B/G6PT-HA
Hep3B/Ctrl
Hep3B/G6PT-HA
Baf. A1
- - + +
M_r(K)
15
LC3
40
HA
40
β-actin
55
p62
40
HA
55
Tubulin
D
Hep3B/Ctrl
Hep3B/G6PT-HA
GFP-LC3 puncta (%)
35
30
25
20
15
10
5
0
**
***
**
Mock
Baf. A1
E
Hep3B/Ctrl
Hep3B/G6PT-HA
GFP
mCherry
Merge
F
GFP+/RFP+
GFP-/RFP+
Number of puncta/cell
40
30
20
10
0
***
**
Hep3B/Ctrl
Hep3B/G6PT-HA

Figure I-6. Beclin1 and ATG5-dependent regulation of G6PT-mediated autophagic flux. (A) Hep3B/Ctrl and Hep3B/G6PT-HA cells were co-transfected with pEGFP-LC3 and pSuper-neo (Ctrl) or Beclin1 shRNA for 72 h. Cell extracts were subjected to western blot analysis (*insert*). (B) The m5-7 cells were left untreated or treated with 10 ng/ml doxycycline for 3 days to induce Atg5 depletion. Cells were then co-transfected with pEGFP-LC3 and pcDNA3-HA (Ctrl) or pG6PT-HA for 24 h. * $P < 0.05$, *** $P < 0.001$.

Figure I-6

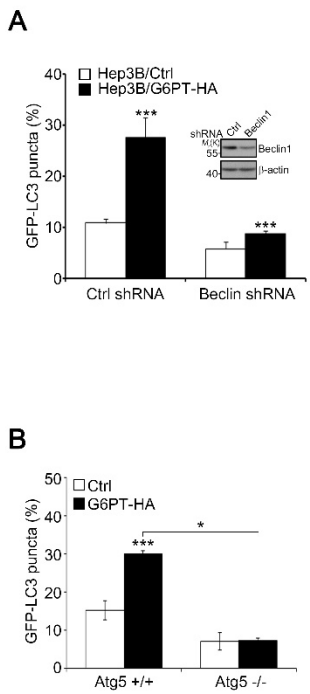
A
Hep3B/Ctrl
Hep3B/G6PT-HA
GFP-LC3 puncta (%)
40
30
20
10
0
***
***
shRNA Ctrl Beclin1
MW
55
40
Beclin1
β-actin
Ctrl shRNA
Beclin shRNA
B
Ctrl
G6PT-HA
GFP-LC3 puncta (%)
50
40
30
20
10
0
*
***
Atg5 +/+
Atg5 -/-

Figure I-7. Reduction of G6PT expression impaired autophagy. (A) Generation of stable G6PT-knockdown Hep3B cells. Hep3B cells were transfected with pSuper-neo (Ctrl) or G6PT shRNAs and selected with 1 mg/ml G418 for 2 weeks. Stable Hep3B/G6PT shRNA cells (#1 and #2) showing reduced expression of G6PT were selected by western blot analysis. (B) Reduced autophagic flux in G6PT-knockdown cells. Hep3B/Ctrl and Hep3B/G6PT shRNA cells (#1 and #2) were left untreated or exposed to 10 nM Bafilomycin A1 (Baf. A1) for 90 min and then analyzed by western blot analysis. (C) Accumulation of p62 in G6PT-knockdown cells. Hep3B/Ctrl and Hep3B/G6PT shRNA cells were grown on coverslips fixed with 4% paraformaldehyde, permeabilized with 0.1% Triton X-100, and stained with anti-p62 antibody (red channel) and Hoechst 33258 (blue channel) for nuclei. Images were acquired using a confocal microscope (*upper*) and the amounts of p62 were quantified (*lower*). Baf. A1-treated Hep3B/Ctrl cells were used as a positive control. * $P < 0.05$. (D) RT-PCR analysis showing p62 mRNA level in G6PT knockdown cells. Total RNA was purified from Hep3B/Ctrl and Hep3B/G6PT shRNA cells and analyzed by reverse transcriptase-polymerase chain reaction (RT-PCR) using gene-specific synthetic primers. Relative intensity of the western blot was measured using ImageJ 1.48v.

Figure I-7

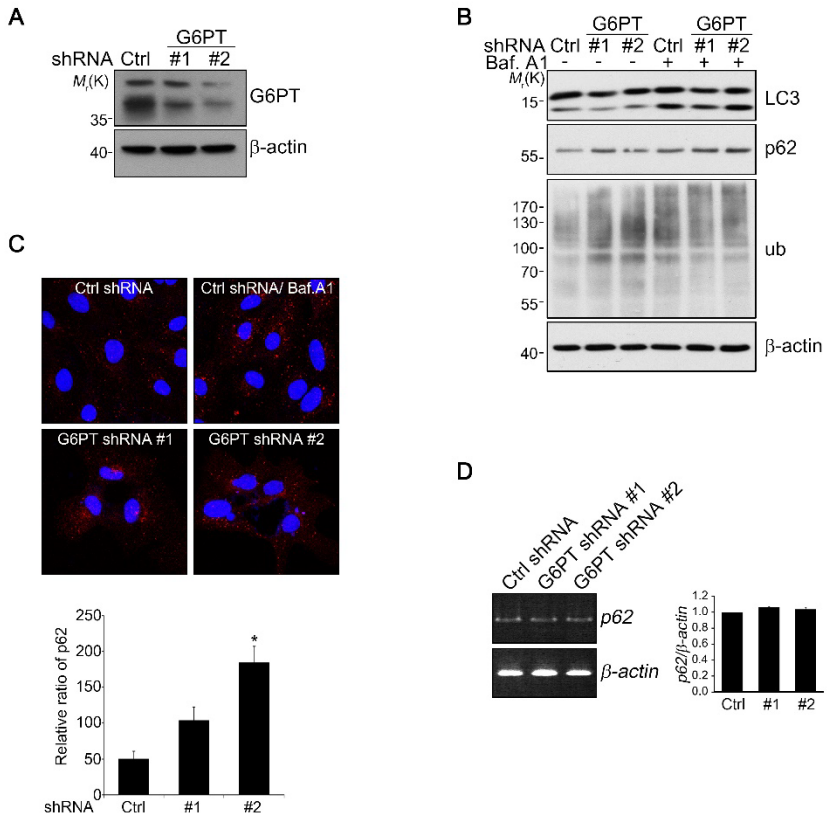
A
shRNA Ctrl G6PT #1 #2
M_r(K)
35
40
G6PT
β-actin
B
shRNA Ctrl G6PT #1 #2 Ctrl G6PT #1 #2
Baf. A1 - - - + + +
M_r(K)
15
55
170
130
100
70
55
40
LC3
p62
ub
β-actin
C
Ctrl shRNA
Ctrl shRNA/ Baf.A1
G6PT shRNA #1
G6PT shRNA #2
Relative ratio of p62
250
200
150
100
50
0
shRNA Ctrl #1 #2
*
D
Ctrl shRNA
G6PT shRNA #1
G6PT shRNA #2
p62
β-actin
p62/β-actin
1.2
1.0
0.8
0.6
0.4
0.2
0.0
Ctrl #1 #2

Figure I-8. Reduction of G6PT increased mutant Huntingtin aggregation. (A and B) Increased aggregation of mutant Huntingtin by G6PT depletion. Hep3B/Ctrl and Hep3B/G6PT shRNA cells were transfected with pHTTex120Q-GFP (mtHTT) for 24 h. Cell lysates were subjected to a filter trap assay and the blots were analyzed by western blotting using anti-GFP antibody. Ponceau S staining was used as loading control (A). HEK293T cells were transfected with pSuper-neo (Ctrl) or G6PT shRNAs for 24 h and further transfected with pHTTex120Q-GFP (mtHTT) for additional 24 h. Cells showing aggregates were counted under a fluorescence microscope (B). ** $P < 0.01$.

Figure I-8

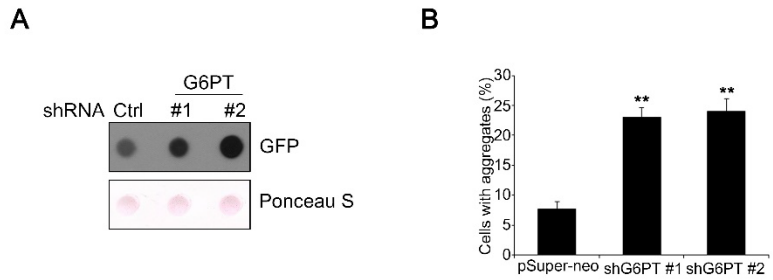
A
G6PT
shRNA Ctrl #1 #2
GFP
Ponceau S
B
Cells with aggregates (%)
30
25
20
15
10
5
0
**
**
pSuper-neo
shG6PT #1
shG6PT #2

Figure I-9. G6PT stimulated autophagy activation independent of its transport activity. (A and B) Effects of G6PT transport activity-dead mutants on autophagy. HEK293T cells were transfected with various G6PT transport activity-dead mutants for 24 h. Cell extracts were analyzed by western blotting (A). Hep3B cells were co-transfected with pEGFP-LC3 and G6PT transport activity-dead mutants for 24 h. Cells showing GFP-LC3 puncta were counted under a fluorescence microscope (B). ** $P < 0.01$, *** $P < 0.001$. (C) Effects of G6PT transport activity-dead mutants on the fluorescence intensity of ULK1-VN/ATG9-VC BiFC. HEK293T cells were co-transfected with pFLAG-ULK1-VN, pHA-ATG9-VC, and pG6PT-HA mutants for 24 h and observed under a fluorescence microscope. The fluorescence intensity of BiFC complex was quantified using Multi Gauge V3.0 (Fuji film). ** $P < 0.01$, *** $P < 0.001$. (D and E) Effects of chlorogenic acid on G6PT-mediated autophagy. HEK293T cells were treated with 1 mM chlorogenic acid (CHA) for 24 h and then treated with 10 nM Bafilomycin A1 (Baf. A1) for additional 2 h. Cell extracts were subjected to western blot analysis (D). Hep3B cells were transfected with pEGFP-LC3 for 16 h and exposed to 1 mM CHA for additional 24 h. Cells showing GFP-LC3 puncta were counted under a fluorescence microscope (E).

Figure I-9

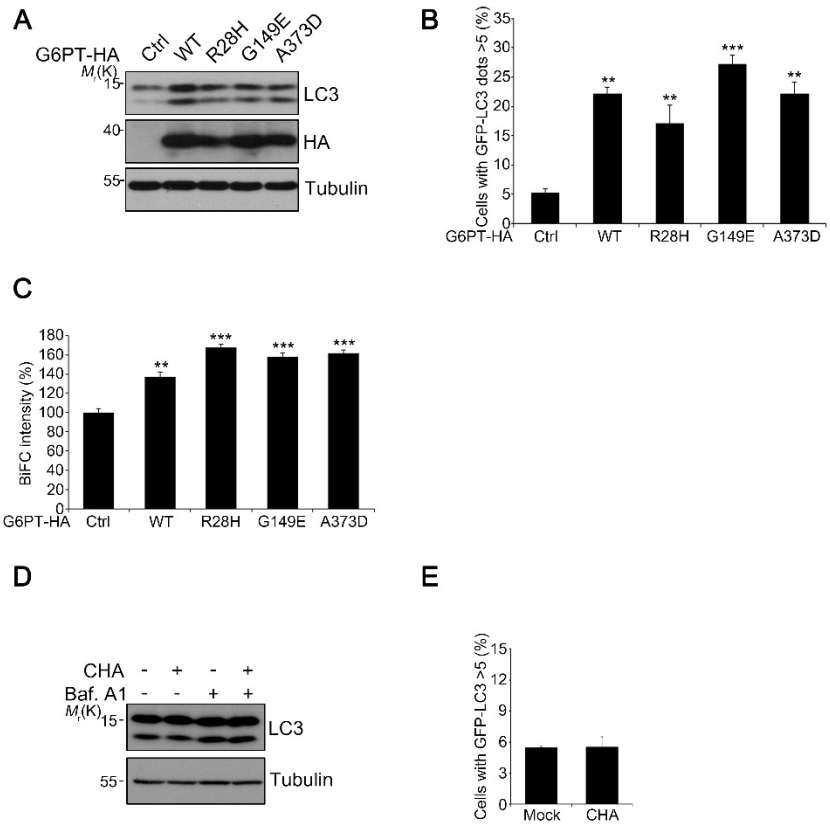
A
G6PT-HA
Ctrl
WT
R28H
G149E
A373D
Mr(K)
15
40
55
LC3
HA
Tubulin
B
Cells with GFP-LC3 dots >5 (%)
35
30
25
20
15
10
5
0
**
**
***
**
G6PT-HA
Ctrl
WT
R28H
G149E
A373D
C
BiFC intensity (%)
180
160
140
120
100
80
60
40
20
0
**
***
***
***
G6PT-HA
Ctrl
WT
R28H
G149E
A373D
D
CHA
Baf. A1
Mr(K)
15
55
LC3
Tubulin
E
Cells with GFP-LC3 >5 (%)
15
12
9
6
3
0
Mock
CHA

Figure I-10. Ectopic expression of G6PT increases autophagic flux in HT22 cells. (A) HT22 cells were co-transfected with pEGFP-LC3 and either pcDNA3-HA (Ctrl) or pG6PT-HA for 24 h. Cells showing GFP-LC3 puncta were counted under a fluorescence microscope. ***$p < 0.001$. (B and C) HT22 cells were transfected with pcDNA-HA (Ctrl) or pG6PT-HA for 24 h and then examined with western blot analysis. (D) HT22 cells were co-transfected with pDFCP1-GFP and either pcDNA-HA (Ctrl) or pG6PT-HA for 24 h. Cells showing DFCP1-GFP puncta (> 10) were counted under a fluorescence microscope. ** $P < 0.01$

Figure I-10

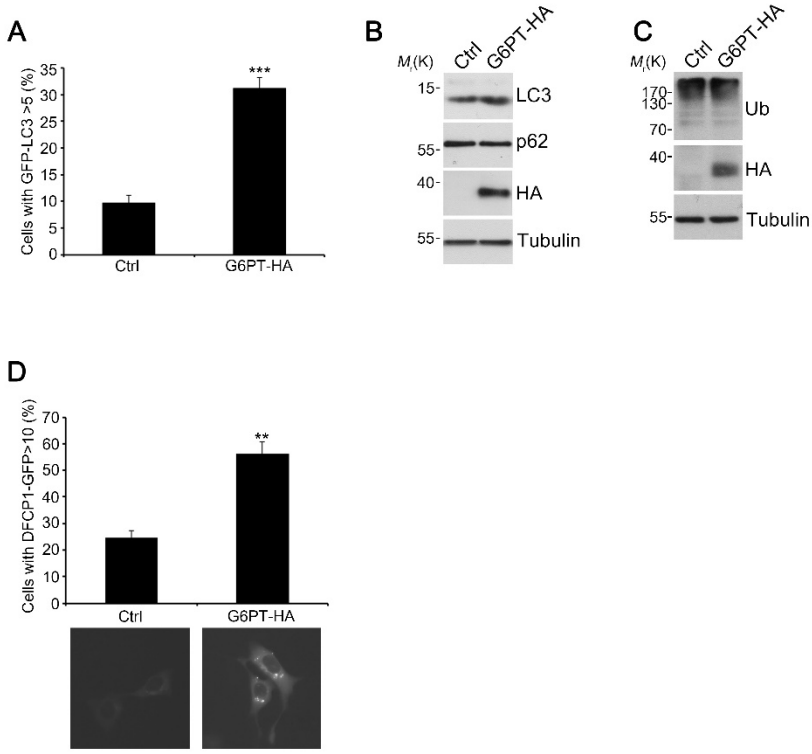
A
Cells with GFP-LC3 >5 (%)
35
30
25
20
15
10
5
0
***
Ctrl
G6PT-HA
B
M_r(K)
Ctrl
G6PT-HA
15-
LC3
55-
p62
40-
HA
55-
Tubulin
C
M_r(K)
Ctrl
G6PT-HA
170-
130-
Ub
70-
40-
HA
55-
Tubulin
D
Cells with DFCP1-GFP>10 (%)
70
60
50
40
30
20
10
0
**
Ctrl
G6PT-HA

Figure I-11. C-terminus of G6PT might function to regulate autophagy. (A) Schematic diagram of G6PT deletion mutants. (B and C) Domain mapping of G6PT for autophagy stimulation. Hep3B cells were co-transfected with pEGFP-LC3 and G6PT deletion mutants for 24 h. Cells with GFP-LC3 puncta were counted under a fluorescence microscope. * $P < 0.05$, *** $P < 0.001$ (B). HEK293T cells were transfected with G6PT-HA deletion mutants for 24 h and then exposed to 5 μM MG132 for additional 6 h. Cell extracts were subjected to western blot analysis (C).

Figure I-11

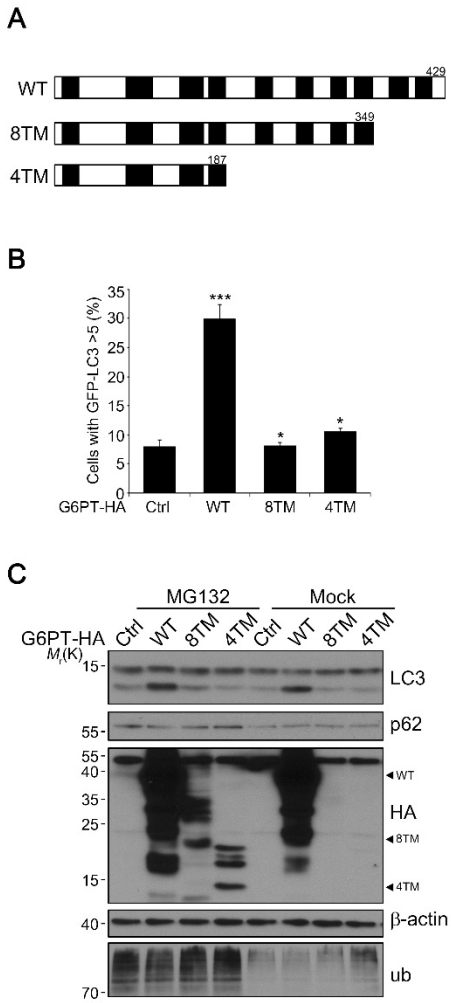
A
WT
8TM
4TM
429
349
187
B
Cells with GFP-LC3 >5 (%)
35
30
25
20
15
10
5
0
***
*
*
G6PT-HA
Ctrl
WT
8TM
4TM
C
MG132
Mock
G6PT-HA
Ctrl
WT
8TM
4TM
Ctrl
WT
8TM
4TM
M_r(K)
15
55
55
40
35
25
15
40
70
LC3
p62
WT
HA
8TM
4TM
β-actin
ub

Figure I-12. Knockdown of G6PT inhibits autophagy activity. (A–C) Decrease of LC3 puncta formation and LC3-II conversion by G6PT knockdown under amino acid starvation. Hep3B/Ctrl and Hep3B/G6PT shRNA cells were incubated with EBSS for 2 h and immunostained with anti-LC3 antibody (A). Hep3B/Ctrl cells and Hep3B/G6PT shRNA cells were transfected with pEGFP-LC3 for 24 h and then incubated with EBSS for additional 2 h. Cells showing GFP-LC3 puncta were counted under a fluorescence microscope. * $P < 0.05$, *** $P < 0.001$ (B). Hep3B/Ctrl and Hep3B/G6PT shRNA cells were exposed to EBSS for 2 h and cell extracts were analyzed by western blotting (C).

Figure I-12

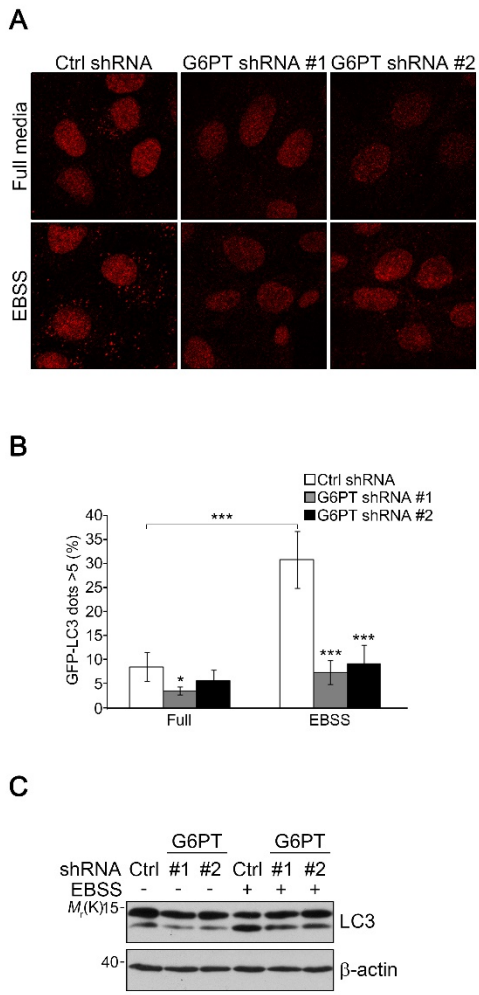
A
Ctrl shRNA
G6PT shRNA #1
G6PT shRNA #2
Full media
EBSS
B
Ctrl shRNA
G6PT shRNA #1
G6PT shRNA #2
GFP-LC3 dots >5 (%)
***
*
***
***
Full
EBSS
C
G6PT
G6PT
shRNA Ctrl #1 #2 Ctrl #1 #2
EBSS - - - + + +
Mr(K)15-
LC3
40-
β-actin

Figure I-13. Knockdown of G6PT expression altered ATG9-GFP distribution. Knockdown of G6PT expression affected sub-cellular distribution of ATG9. Hep3B/Ctrl and Hep3B/G6PT shRNA cells were transfected with pATG9-EGFP for 24 h and then incubated with EBSS for 2 h. Cells showing ATG9-GFP puncta were counted under a fluorescence microscope (A and B). ** $P < 0.01$, *** $P < 0.001$.

Figure I-13

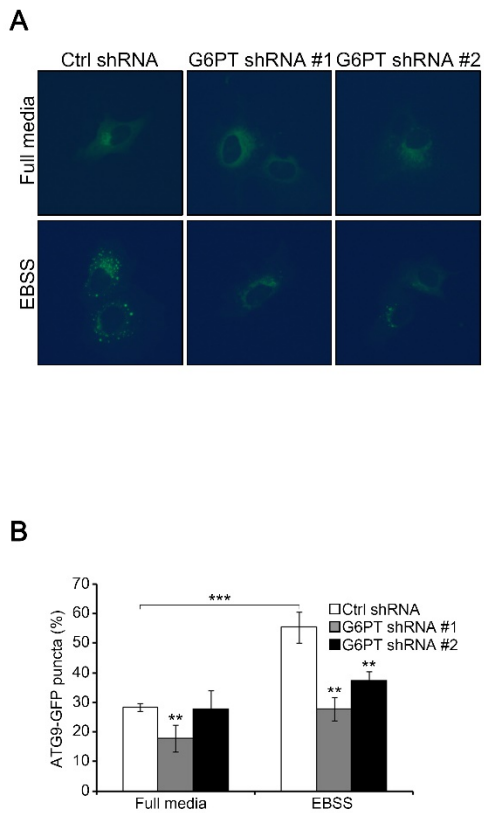
A
Ctrl shRNA
G6PT shRNA #1
G6PT shRNA #2
Full media
EBSS
B
ATG9-GFP puncta (%)
70
60
50
40
30
20
10
0
***
**
**
**
Ctrl shRNA
G6PT shRNA #1
G6PT shRNA #2
Full media
EBSS

Figure I-14. G6PT activated autophagy by inhibiting mTORC1 during amino acid starvation. (A) Increase of mTORC1 activity by G6PT depletion. Hep3B/Ctrl and Hep3B/G6PT shRNA cells were exposed to EBSS for 2 h and subjected to western blot analysis. short, short exposure; long, long exposure. Relative intensity of the western blot was measured using ImageJ 1.48v. (B) Hep3B/Ctrl and Hep3B/G6PT shRNA cells were either left untreated or treated Rapamycin (0.1 μg/ml) for 6 h. Cell extracts were analyzed by western blot analysis. (C) Enhanced phosphorylation of ULK1 in G6PT depleted cells. Hep3B/Ctrl and Hep3B/G6PT shRNA cells were exposed to either full medium or EBSS for 2 h. Cells were then analyzed by western blot analysis using indicated antibodies.

Figure I-14

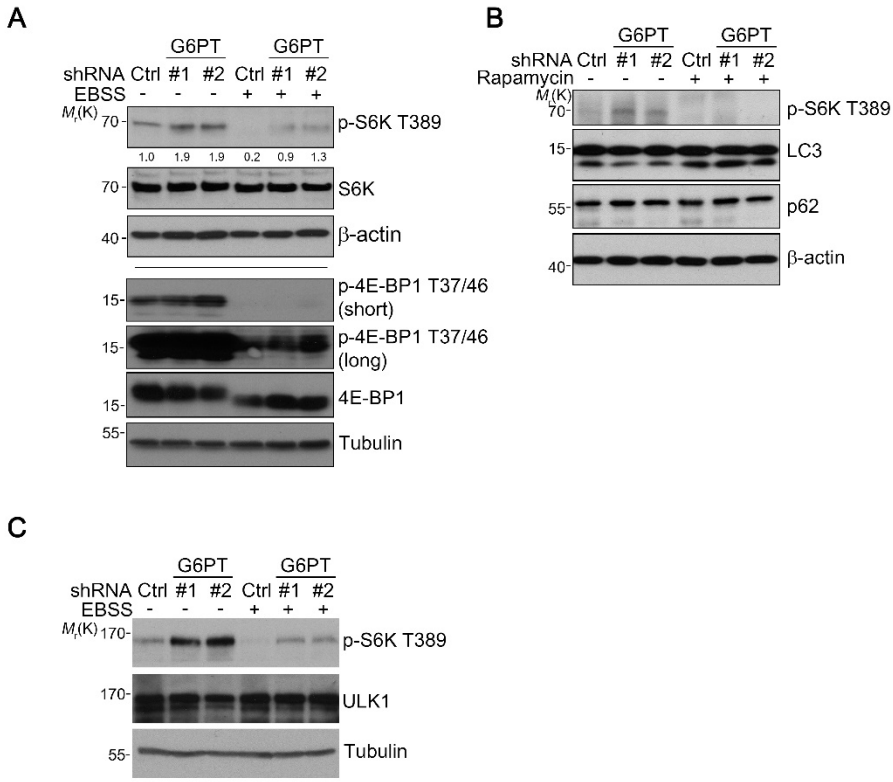
A
G6PT
G6PT
shRNA Ctrl #1 #2 Ctrl #1 #2
EBSS - - - + + +
Mr(K)
70
p-S6K T389
1.0 1.9 1.9 0.2 0.9 1.3
70
S6K
40
β-actin
15
p-4E-BP1 T37/46 (short)
15
p-4E-BP1 T37/46 (long)
15
4E-BP1
55
Tubulin
B
G6PT
G6PT
shRNA Ctrl #1 #2 Ctrl #1 #2
Rapamycin - - - + + +
Mr(K)
70
p-S6K T389
15
LC3
55
p62
40
β-actin
C
G6PT
G6PT
shRNA Ctrl #1 #2 Ctrl #1 #2
EBSS - - - + + +
Mr(K)
170
p-S6K T389
170
ULK1
55
Tubulin

Figure I-15. Down regulation of G6PT inhibits glucose starvation-induced autophagy by activating AMPK. (A and B) Suppression of AMPK activity by G6PT knockdown under glucose depletion. Hep3B/Ctrl and Hep3B/G6PT shRNA cells were exposed to glucose-free medium for 2 h and subjected to western blot analysis. Relative intensity of the western blot was measured using ImageJ 1.48v (A). Hep3B/Ctrl and Hep3B/G6PT shRNA cells were transfected with pEGFP-LC3 for 24 h and incubated with glucose-free medium for additional 2 h. Cells showing GFP-LC3 puncta were counted under a fluorescence microscope (B). ** $P < 0.01$, *** $P < 0.001$. (C) Effects of G6PT-HA deletion mutants on mTORC1 activity. HEK293T cells were transfected with G6PT transport activity-dead mutants for 24 h. Cell extracts were analyzed by western blotting using indicated antibodies.

Figure I-15

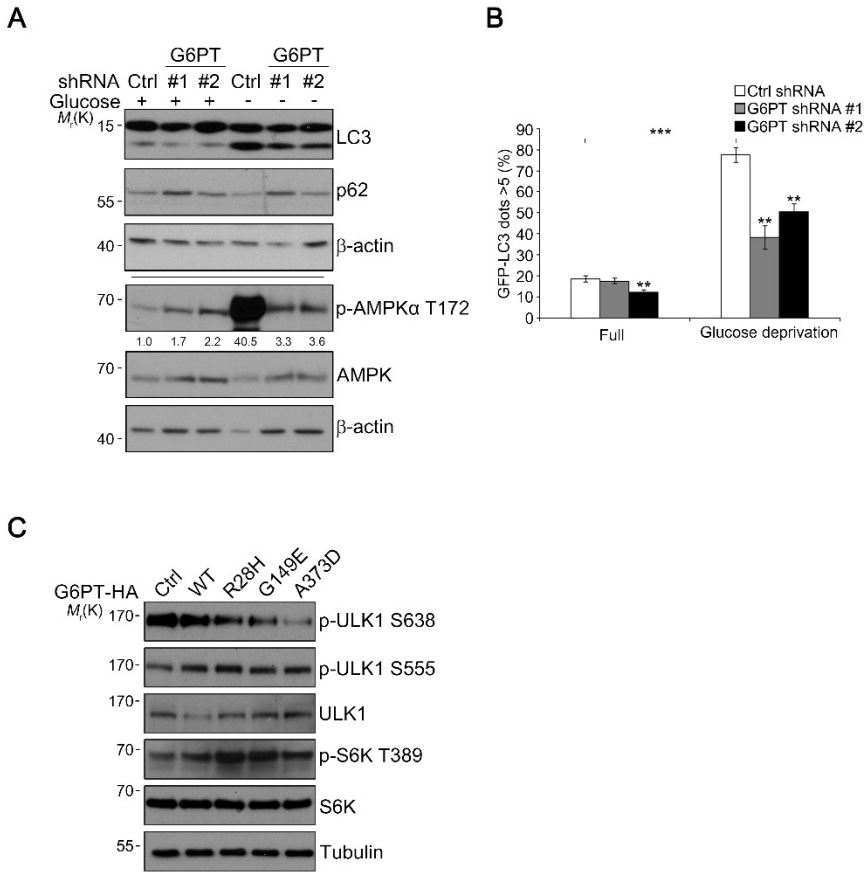
A
G6PT
G6PT
shRNA Ctrl #1 #2 Ctrl #1 #2
Glucose + + + - - -
M_r(K)
15
LC3
55
p62
40
β-actin
70
p-AMPKα T172
1.0 1.7 2.2 40.5 3.3 3.6
70
AMPK
40
β-actin
B
Ctrl shRNA
G6PT shRNA #1
G6PT shRNA #2
GFP-LC3 dots >5 (%)
90
80
70
60
50
40
30
20
10
0
***
**
**
**
Full
Glucose deprivation
C
G6PT-HA Ctrl WT R28H G149E A373D
M_r(K)
170
p-ULK1 S638
170
p-ULK1 S555
170
ULK1
70
p-S6K T389
70
S6K
55
Tubulin

Discussion

In this study, I aimed to identify new regulators functioning at the initiation stage of autophagy. Based on a recent study showing a functional and physical interaction between Atg1, an ULK1 homolog, and Atg9 in yeast (Sekito et al., 2009), I developed a functional screening assay using the BiFC system to detect autophagy activation. Compared with the LC3 measurement assays, the BiFC assay using ULK1-VN and ATG9-VC provides an advantage in that fluorescence signal is generated only by autophagy activation but not autophagy inhibition, thus facilitating the successful identification of autophagy activators from a cDNA library. In particular, this assay is a viable method in monitoring the initiation step of autophagy upstream of ULK1 and ATG9.

Similar to the case in yeast and *Drosophila*, I observed the protein-protein interactions between ULK1 and ATG9 in mammalian cells with immunoprecipitation assays. Unlike in BiFC assays in which autophagy stimuli increased the fluorescence, I could not find convincing evidence showing that the interaction between endogenous ULK1 and ATG9 was regulated during autophagy in mammalian cells. In yeast, Atg1 has been shown to regulate Atg9 through their association (Sekito et al., 2009). The

absence of regulated interaction between endogenous ULK1 and ATG9 in mammalian cells may arise from a difference in the mode of interaction between ULK1 and ATG9 in yeast and mammalian cells. Alternatively, it may be easier to observe the regulated interaction between ULK1 and ATG9 in the BiFC assay than in the immunoprecipitation assay, since the interaction in the BiFC assay is irreversible (Kodama and Hu, 2012). Therefore, the mode of interaction between ULK1 and ATG9 in mammalian cells, whether direct or indirect, remains to be further elucidated.

Although G6PT serves to transport G6P into the ER lumen during the cascade of gluconeogenesis or glycogenolysis to produce glucose, I could not observe any positive relationship between the transport activities of G6PT and autophagy. Accumulating evidence has implied that G6PT may have functions other than glucose production. First, G6PT is expressed all over the organ whereas G6Pase-α is only expressed in the liver and kidney. Second, GSD1b patients who carry G6PT mutations exhibit different symptoms from GSD1a patients who bear G6Pase malfunction. In addition to disruption of glucose homeostasis, GSD1b patients show neutropenia (Gitzelmann and Bosshard, 1993). Interestingly, although GSD1b patients have the same mutation in G6PT gene, the severity of neutropenia in the patients and their corresponding therapies are different (Melis et al., 2005). Recently, a *G6pt*$^{-/-}$ mouse model was developed to study the potential roles of G6PT beyond

glucose homeostasis in neutrophil cells. While *G6pt*$^{-/-}$ mice show same phenotype as G6Pase deficiency which is characterized by growth retardation, hypoglycemia, hepatomegaly, and nephromegaly, *G6pt*$^{-/-}$ mice also showed myeloid dysfunction, altered hematopoiesis in the bone marrow and spleen, abnormal chemokine production and impaired calcium flux in neutrophils (Chen et al., 2003). Although a number of studies are in progress, the relationship between neutropenia severity and transport activity of G6PT has not been clearly revealed. For these reasons, I suggest that the autophagy-stimulatory activity of G6PT independent of its transport activity may be one of the additional functions of G6PT. I therefore encourage further investigation in identifying the functions of G6PT in autophagy and neutropenia on GSD1b patients.

In this study, G6PT-mTORC1 signaling is essential in promoting autophagy in hepatic cell line. Malfunction of mTORC1 is frequently associated with metabolic diseases, including type 2 diabetes and cancer (Zoncu et al., 2011). Additionally, high levels of glucose in hepatic cells due to uncontrolled G6PT expression is widely observed in type 2 diabetic patients (Foster and Nordlie, 2002). Our observation that G6PT regulates mTORC1 and autophagy may provide a new way to interpret the role of G6PT in metabolic syndromes. In addition, G6PT is localized to the ER membrane whereas activated mTORC1 is found in the lysosome. Therefore, a question

remains as to how G6PT regulates mTORC1. One possible explanation is that G6PT regulates mTORC1 through calcium mobilization, because a recent study has revealed that knockdown of G6PT expression disrupts calcium mobilization in glioblastoma cells (Chen et al., 2003). Consistently, mTORC1 is regulated by VPS34 in a calcium channel-dependent manner in the lysosome (Gulati et al., 2008). Especially, our observation that G6PT regulates AMPK during glucose starvation-induced autophagy suggests a pivotal role of G6PT in the regulation of mTORC1 through AMPK. AMPK is an energy sensor activated in response to increased cellular AMP, ADP or Ca^{2+} level and is phosphorylated by LKB1 and Ca^{2+}/calmodulin-activated protein kinase β (CaMKKβ) (Mihaylova and Shaw, 2011). Because AMPK regulates autophagy through either direct phosphorylation of ULK1 or inhibition of mTORC1 (Hawley et al., 2005), disruption of calcium mobilization caused by G6PT dysfunction might affect both AMPK and mTORC1, resulting in inhibition of autophagy.

In conclusion, I have established a functional screening assay using the BiFC system to study the interaction between ULK1 and ATG9. This assay enabled us to identify G6PT as a specific modulator of the initiation step of autophagy.

References

Bellot, G., Garcia-Medina, R., Gounon, P., Chiche, J., Roux, D., Pouyssegur, J., and Mazure, N.M. (2009). Hypoxia-induced autophagy is mediated through hypoxia-inducible factor induction of BNIP3 and BNIP3L via their BH3 domains. Molecular and cellular biology *29*, 2570-2581.

Chen, L.Y., Shieh, J.J., Lin, B., Pan, C.J., Gao, J.L., Murphy, P.M., Roe, T.F., Moses, S., Ward, J.M., Lee, E.J., *et al.* (2003). Impaired glucose homeostasis, neutrophil trafficking and function in mice lacking the glucose-6-phosphate transporter. Human molecular genetics *12*, 2547-2558.

Chen, S.Y., Pan, C.J., Lee, S., Peng, W., and Chou, J.Y. (2008a). Functional analysis of mutations in the glucose-6-phosphate transporter that cause glycogen storage disease type Ib. Molecular genetics and metabolism *95*, 220-223.

Chen, S.Y., Pan, C.J., Nandigama, K., Mansfield, B.C., Ambudkar, S.V., and Chou, J.Y. (2008b). The glucose-6-phosphate transporter is a phosphate-linked antiporter deficient in glycogen storage disease type Ib and Ic. FASEB journal : official publication of the Federation of American Societies for Experimental Biology *22*, 2206-2213.

Feng, Y., He, D., Yao, Z., and Klionsky, D.J. (2014). The machinery of macroautophagy. Cell research *24*, 24-41.

Foster, J.D., and Nordlie, R.C. (2002). The biochemistry and molecular biology of the glucose-6-phosphatase system. Experimental biology and medicine (Maywood, NJ) *227*, 601-608.

Froissart, R., Piraud, M., Boudjemline, A.M., Vianey-Saban, C., Petit, F., Hubert-Buron, A., Eberschweiler, P.T., Gajdos, V., and Labrune, P. (2011). Glucose-6-phosphatase deficiency. Orphanet journal of rare diseases *6*, 27.

Ganley, I.G., Lam du, H., Wang, J., Ding, X., Chen, S., and Jiang, X. (2009). ULK1.ATG13.FIP200 complex mediates mTOR signaling and is essential for autophagy. The Journal of biological chemistry *284*, 12297-12305.

Gitzelmann, R., and Bosshard, N.U. (1993). Defective neutrophil and monocyte functions in glycogen storage disease type Ib: a literature review. European journal of pediatrics *152 Suppl 1*, S33-38.

Gulati, P., Gaspers, L.D., Dann, S.G., Joaquin, M., Nobukuni, T., Natt, F., Kozma, S.C., Thomas, A.P., and Thomas, G. (2008). Amino acids activate mTOR complex 1 via Ca2+/CaM signaling to hVps34. Cell metabolism *7*, 456-465.

Hara, T., Nakamura, K., Matsui, M., Yamamoto, A., Nakahara, Y., Suzuki-Migishima, R., Yokoyama, M., Mishima, K., Saito, I., Okano, H., *et al.* (2006). Suppression of basal autophagy in neural cells causes neurodegenerative

disease in mice. Nature *441*, 885-889.

Hawley, S.A., Pan, D.A., Mustard, K.J., Ross, L., Bain, J., Edelman, A.M., Frenguelli, B.G., and Hardie, D.G. (2005). Calmodulin-dependent protein kinase kinase-beta is an alternative upstream kinase for AMP-activated protein kinase. Cell metabolism *2*, 9-19.

Hosokawa, N., Hara, Y., and Mizushima, N. (2006). Generation of cell lines with tetracycline-regulated autophagy and a role for autophagy in controlling cell size. FEBS letters *580*, 2623-2629.

Hosokawa, N., Sasaki, T., Iemura, S., Natsume, T., Hara, T., and Mizushima, N. (2009). Atg101, a novel mammalian autophagy protein interacting with Atg13. Autophagy *5*, 973-979.

Ichimura, Y., Kumanomidou, T., Sou, Y.S., Mizushima, T., Ezaki, J., Ueno, T., Kominami, E., Yamane, T., Tanaka, K., and Komatsu, M. (2008). Structural basis for sorting mechanism of p62 in selective autophagy. The Journal of biological chemistry *283*, 22847-22857.

Inoki, K., Zhu, T., and Guan, K.L. (2003). TSC2 mediates cellular energy response to control cell growth and survival. Cell *115*, 577-590.

Itakura, E., and Mizushima, N. (2010). Characterization of autophagosome formation site by a hierarchical analysis of mammalian Atg proteins. Autophagy *6*, 764-776.

Jiang, P., and Mizushima, N. (2014). Autophagy and human diseases. Cell

research *24*, 69-79.

Jung, C.H., Jun, C.B., Ro, S.H., Kim, Y.M., Otto, N.M., Cao, J., Kundu, M., and Kim, D.H. (2009). ULK-Atg13-FIP200 complexes mediate mTOR signaling to the autophagy machinery. Molecular biology of the cell *20*, 1992-2003.

Kesidou, E., Lagoudaki, R., Touloumi, O., Poulatsidou, K.N., and Simeonidou, C. (2013). Autophagy and neurodegenerative disorders. Neural regeneration research *8*, 2275-2283.

Kim, J., Kundu, M., Viollet, B., and Guan, K.L. (2011). AMPK and mTOR regulate autophagy through direct phosphorylation of Ulk1. Nature cell biology *13*, 132-141.

Kodama, Y., and Hu, C.D. (2012). Bimolecular fluorescence complementation (BiFC): a 5-year update and future perspectives. BioTechniques *53*, 285-298.

Kouroku, Y., Fujita, E., Tanida, I., Ueno, T., Isoai, A., Kumagai, H., Ogawa, S., Kaufman, R.J., Kominami, E., and Momoi, T. (2007). ER stress (PERK/eIF2alpha phosphorylation) mediates the polyglutamine-induced LC3 conversion, an essential step for autophagy formation. Cell death and differentiation *14*, 230-239.

Koyama-Honda, I., Itakura, E., Fujiwara, T.K., and Mizushima, N. (2013). Temporal analysis of recruitment of mammalian ATG proteins to the

autophagosome formation site. Autophagy *9*, 1491-1499.

Lee, H., Noh, J.Y., Oh, Y., Kim, Y., Chang, J.W., Chung, C.W., Lee, S.T., Kim, M., Ryu, H., and Jung, Y.K. (2012). IRE1 plays an essential role in ER stress-mediated aggregation of mutant huntingtin via the inhibition of autophagy flux. Human molecular genetics *21*, 101-114.

Ma, X.M., and Blenis, J. (2009). Molecular mechanisms of mTOR-mediated translational control. Nature reviews Molecular cell biology *10*, 307-318.

Matsui, A., Kamada, Y., and Matsuura, A. (2013). The role of autophagy in genome stability through suppression of abnormal mitosis under starvation. PLoS Genet *9*, e1003245.

Melis, D., Fulceri, R., Parenti, G., Marcolongo, P., Gatti, R., Parini, R., Riva, E., Della Casa, R., Zammarchi, E., Andria, G., *et al.* (2005). Genotype/phenotype correlation in glycogen storage disease type 1b: a multicentre study and review of the literature. European journal of pediatrics *164*, 501-508.

Mihaylova, M.M., and Shaw, R.J. (2011). The AMPK signalling pathway coordinates cell growth, autophagy and metabolism. Nature cell biology *13*, 1016-1023.

Nazio, F., Strappazzon, F., Antonioli, M., Bielli, P., Cianfanelli, V., Bordi, M., Gretzmeier, C., Dengjel, J., Piacentini, M., Fimia, G.M., *et al.* (2013). mTOR inhibits autophagy by controlling ULK1 ubiquitylation, self-association and

function through AMBRA1 and TRAF6. Nature cell biology *15*, 406-416.

Nishida, Y., Arakawa, S., Fujitani, K., Yamaguchi, H., Mizuta, T., Kanaseki, T., Komatsu, M., Otsu, K., Tsujimoto, Y., and Shimizu, S. (2009). Discovery of Atg5/Atg7-independent alternative macroautophagy. Nature *461*, 654-658.

Nixon, R.A. (2013). The role of autophagy in neurodegenerative disease. Nature medicine *19*, 983-997.

Pan, C.J., Chen, S.Y., Lee, S., and Chou, J.Y. (2009). Structure-function study of the glucose-6-phosphate transporter, an eukaryotic antiporter deficient in glycogen storage disease type Ib. Molecular genetics and metabolism *96*, 32-37.

Puri, C., Renna, M., Bento, C.F., Moreau, K., and Rubinsztein, D.C. (2014). ATG16L1 meets ATG9 in recycling endosomes: additional roles for the plasma membrane and endocytosis in autophagosome biogenesis. Autophagy *10*, 182-184.

Pyo, J.O., Yoo, S.M., Ahn, H.H., Nah, J., Hong, S.H., Kam, T.I., Jung, S., and Jung, Y.K. (2013). Overexpression of Atg5 in mice activates autophagy and extends lifespan. Nature communications *4*, 2300.

Rouschop, K.M., van den Beucken, T., Dubois, L., Niessen, H., Bussink, J., Savelkouls, K., Keulers, T., Mujcic, H., Landuyt, W., Voncken, J.W., *et al.* (2010). The unfolded protein response protects human tumor cells during hypoxia through regulation of the autophagy genes MAP1LC3B and ATG5.

The Journal of clinical investigation *120*, 127-141.

Russell, R.C., Yuan, H.X., and Guan, K.L. (2014). Autophagy regulation by nutrient signaling. Cell research *24*, 42-57.

Sancak, Y., Bar-Peled, L., Zoncu, R., Markhard, A.L., Nada, S., and Sabatini, D.M. (2010). Ragulator-Rag complex targets mTORC1 to the lysosomal surface and is necessary for its activation by amino acids. Cell *141*, 290-303.

Sekito, T., Kawamata, T., Ichikawa, R., Suzuki, K., and Ohsumi, Y. (2009). Atg17 recruits Atg9 to organize the pre-autophagosomal structure. Genes to cells : devoted to molecular & cellular mechanisms *14*, 525-538.

Talloczy, Z., Jiang, W., Virgin, H.W.t., Leib, D.A., Scheuner, D., Kaufman, R.J., Eskelinen, E.L., and Levine, B. (2002). Regulation of starvation- and virus-induced autophagy by the eIF2alpha kinase signaling pathway. Proceedings of the National Academy of Sciences of the United States of America *99*, 190-195.

Tang, H.W., Liao, H.M., Peng, W.H., Lin, H.R., Chen, C.H., and Chen, G.C. (2013). Atg9 interacts with dTRAF2/TRAF6 to regulate oxidative stress-induced JNK activation and autophagy induction. Developmental cell *27*, 489-503.

Yang, Z., and Klionsky, D.J. (2010). Eaten alive: a history of macroautophagy. Nature cell biology *12*, 814-822.

Young, A.R., Chan, E.Y., Hu, X.W., Kochl, R., Crawshaw, S.G., High, S.,

Hailey, D.W., Lippincott-Schwartz, J., and Tooze, S.A. (2006). Starvation and ULK1-dependent cycling of mammalian Atg9 between the TGN and endosomes. Journal of cell science *119*, 3888-3900.

Zoncu, R., Efeyan, A., and Sabatini, D.M. (2011). mTOR: from growth signal integration to cancer, diabetes and ageing. Nature reviews Molecular cell biology *12*, 21-35.

CHAPTER II

Identification of ZAK as an essential autophagy regulator

Abstract

Autophagy is a cellular degradation system for maintaining cellular homeostasis under various stress signals such as nutrient deprivation, hypoxic condition, or endoplasmic reticulum stress. To overcome the stress conditions, cells utilize autophagy-specific proteins to generate double-membrane vesicle called autophagosome to sequester cytosolic components and subcellular organelles to fuse with lysosome. However, molecular detail for the regulation of autophagy initiation under stress condition is not fully understood. Here, I show that ZAK kinase is an essential regulator of basal and induced autophagy. I first established ATG7-VN/VCn-ATG12 bimolecular fluorescence complementation (BiFC) cell-based assay to isolate autophagy modulators which regulate interaction between ATG7, an E1-like activating enzyme, and ATG12. Utilizing the assay, I performed gain-of-function screening of 900 cDNAs which encode mammalian kinases and phosphatases, and isolated ZAK as a potent autophagy activator. Ectopic expression of ZAK enhanced the fluorescence of ATG7-VN/VCn-ATG12 BiFC assay and increased the interaction between them. Overexpression of ZAK reduced the levels of p62 and ubiquitin conjugates but increased LC3 dot formation, leading to increase of autophagy flux, while ZAK K45M

kinase-dead mutant failed to do so. Conversely, knockdown of ZAK expression inhibited basal autophagy. Interestingly, down-regulation of ZAK blocked amino acid or serum starvation-induced autophagy to almost to control level. Furthermore, I found that ZAK interacted with ATG7 in cells. I hypothesize that ZAK is an essential regulator of autophagy which functions through its kinase activity and interaction with ATG7.

Introduction

Autophagy is a cellular process that cytosolic components are destined to lysosome for its degradation (Ohsumi, 2014). Autophagy is classified by its degrading targets; mitophagy is mitochondrial degradation by autophagy (Kim et al., 2007; Youle and Narendra, 2011), pexophagy is for peroxisome-selective degradation (Dunn et al., 2005). Xenophagy is named for bacteria and virus clearance, while aggrephagy is degradation of protein aggregates such as polyQ-huntingtin (Randow and Munz, 2012; Yamamoto and Simonsen, 2011). Autophagy is also categorized according to its mechanism; macroautophagy, microautophagy, and chaperone-mediated autophagy (CMA). Unfolded substrates are directly translocated by CMA process across the lysosome membrane with the help of cytosolic, lysosomal chaperone HSC70 and the integral membrane receptor lysosomal-associated membrane protein type 2A (LAMP-2A) (Cuervo and Dice, 1996). Microautophagy, relatively less studied, is a process in which portion of cytoplasm or organelles are directly sequestered by invagination of lysosomal membrane and subsequently engulfed by lysosome (Kunz et al., 2004; Li et al., 2012). Macroautophagy (hereafter autophagy), on the other hand, sequesters its cargoes within a unique double-membrane structure called an

autophagosome (Ohsumi, 2014). To generate autophagosome, several autophagy-related proteins (ATGs) are assembled to form phagophore. Then, concerted actions of ATGs function to expand and closure of phagophore to generate autophagosome (Feng et al., 2014).

Among the ATGs, two ubiquitin-like systems are participated in autophagosomal membrane biogenesis and membrane expansion steps (Geng and Klionsky, 2008; Nakatogawa, 2013). Defects in the recruitment of ubiquitin-like proteins (UBLs) proteins to the expanding phagophore does not affect autophagosomal initiation step but fails to closure of autophagosome. These reports demonstrate that the two conjugation systems participate in the membrane expansion. Two ubiquitin-like proteins (UBLs), LC3 and ATG12, are first conjugated to E1 enzyme, ATG7, and transferred to ATG3 or ATG10, E2 enzymes. Then, ATG12 is eventually attached to ATG5 via isopeptide bond, while LC3 is conjugated to phosphatidylethanolamine (PE). For ATG12-ATG5 conjugation, E3 enzyme activity does not required since ATG5 is directly recognized by E2 enzyme ATG10 (Yamaguchi et al., 2012b). Finally, ATG12-ATG5 conjugate binds to ATG16L1 with noncovalent bond that drives oligomerization of the ternary complexes. Unlike ATG12-ATG5 conjugates, LC3-PE conjugate requires E3 enzyme activity that is function of ATG12-ATG5-ATG16L (Fujita et al., 2008). ATG12-ATG5-ATG16L1 complex localizes on the expanding phagophore and is dissociated from the

membrane after the completion of autophagosome formation while LC3-PE is resided both inner and outer surface of the phagophore and remained on the inner surface after the membrane completion (Weidberg et al., 2010).

ATG7, an E1-like enzyme for both ATG12 and LC3, has distinctive three functional domains. The N-terminal domain functions to recruit ATG3 or ATG10 (Kaiser et al., 2012; Yamaguchi et al., 2012a). The C-terminal domain is required for its E1 activity and has roles in binding with substrates (Noda et al., 2011; Taherbhoy et al., 2011). The central domain of ATG7, adenylation domain, has several important main functions. First of all, the domain binds to UBL and Mg-ATP and catalyzes UBL activation. Second, it mediates homodimerization of ATG7 itself. Third, the central domain of ATG7 functions in the formation of thioester-linked ATG7-UBL intermediate. Last, this domain delivers the UBL's C-terminus to its E2s (Hong et al., 2011; Komatsu et al., 2001). However, its regulation remains elusive.

Since autophagy is tightly connected with human diseases and regulating autophagosome formation is a key mechanism, ATG proteins which belong to ubiquitin-like conjugation systems can be potential pharmacological target. ATG5 or ATG7 knockout mice were shown that autophagy is crucial for survival during neonatal starvation (Komatsu et al., 2005; Kuma et al., 2004). According to studies in neurodegenerative disease, the function of autophagy is well characterized. In sporadic Parkinson's

disease, altered expressions of ATG5 and ATG7 have been reported. Moreover, mutation in ATG7 has been informed to be associated with earlier onset of Huntington's disease. (Chen et al., 2013; Metzger et al., 2010). Autophagy also contributes to immune responses. Not only autophagy directly engulfs and degrades pathogens, but also it mediates antigen presentation. In addition, down-regulation of ATG5 expression level increases susceptibility to bacterial infection (Nakagawa et al., 2004). Moreover, ATG12-ATG5-ATG16L1 complexes are needed for IFN-gamma-mediated antiviral function. Mutation of ATG16L1 is tightly associated with Crohn's disease caused by defective immunity (Hampe et al., 2007; Hwang et al., 2012; Saitoh et al., 2008).

ZAK (sterile alpha motif and leucine zipper containing kinase AZK) belongs to the member of the MAPKK kinase (MAPKKK) family (Gallo and Johnson, 2002). There are two spliced forms of ZAK; ZAK-α is a longest form and ZAK-β is generated by alternative splicing with C-terminal truncation. ZAK contains several domains including N-terminal kinase catalytic domain, leucine zipper motif, and sterile-α motif (SAM). N-terminus of ZAK-β is identical to ZAK-α but has incomplete SAM domain (Gotoh et al., 2001). ZAK is mainly located on cytosol and binds to magnesium for homodimer formations. Studies on ZAK identified that ZAK suppresses cell proliferation (Yang et al., 2010). Moreover, it increases G2/M phase of cell

population, while expression of dominant-negative form of ZAK attenuates the G2 arrest by gamma-radiation (Gross et al., 2002). Also, overexpression of ZAK enhances LPA-stimulated invasion through direct binding with GTP-bounded RhoA and RhoC (Korkina et al., 2013). ZAK regulates stress signal through extracellular signal-regulated kinase (ERK) or c-Jun N-terminal kinase (JNK). Lots of product associated with oncogenesis or tumorigenesis including MAPK/ERK have been reported to affect autophagy signaling. Ras-Raf-MEK-ERK pathway is a chain of proteins that shares a signal from a small G protein receptor on the cell surface. Conversely, ZAK regulates stress signal through extracellular signal-regulated kinase (ERK) or c-Jun N-terminal kinase (JNK) (Yang et al., 2010). However, its function in autophagy is not yet known.

In this study, I isolated ZAK from functional screening as a potential regulator of autophagy. I propose that ZAK functions to regulate autophagy through its kinase activity and interacting with ATG7.

Materials and methods

DNA Constructs

The cDNA of ATG7 was amplified by PCR using synthetic oligonucleotides (forward 5′-CCG GGG TAC CCC GGG CGG CAG CTA CGG GGG-3′ and reverse 5′-GGG GTA CCC CGA TGG TCT CAT CAT CGC TC-3′). The amplified product was subcloned into *Kpn*I site of pFLAG-VN173. To generate VCn-HA-ATG12, ATG12 cDNA was amplified by PCR using synthetic oligonucleotides (forward 5′-CCG CTC GAG CGG GCG GAG GAG CCG CAG TC-3′ and reverse 5′-CCG CTC GAG CGG TCA TCC CCA CGC CTG AGA CTT G-3′) and subcloned into *Xho*I site of pcDNA3-HA. Then, amplified product of VC155 (forward 5′-CCC AAG CTT GGG ATG TAC CCA TAC GAT GTT C-3′ and reverse 5′-CCC AAG CTT GGG CTT GTA CAG CTC GTC CAT G-3′) was subcloned into *Hin*dIII site of pHA-ATG12. The cDNA of ZAK was amplified by PCR using synthetic oligonucleotides (forward 5′-CCG CTC GAA CGG TCG TCT CTC GGT GCC TCC-3′ and reverse 5′-GGG GTA CCC CTC ATT CAC TAT TAT CCA TGT C-3′) and subcloned into *Xho*I/*Kpn*I site of pEGFP-C1. ZAK shRNAs were constructed using forward and reverse synthetic 19-base sequences (#1,

5′-$_{921}$GCT TAA AGA ACG AGA AAG A-3′; #2, 5′-$_{1010}$GAA TGT CTG AGG AGT CTT A-3′), which were cloned into *Bgl*II/*Hin*dIII sites of pSuper-neo (Oligoengine).

Cell Culture and DNA Transfection

HEK293T (human embryonic kidney) cells were cultured in DMEM supplemented with 10% fetal bovine serum (FBS) (Hyclone), penicillin, and streptomycin (Invitrogen). Hep3B (human hepatocellular carcinoma) cells were maintained in RPMI 1640 (Hyclone) supplemented with 10% FBS. Cells were cultured at 37°C under an atmosphere of 5% CO_2. Transfection was carried out using Polyfect reagent (Qiagen) or PEI (Sigma) according to the manufacturer's instructions.

BiFC Assay for cDNA Library Screening

HEK 293T cells grown in a 96-well plate were co-transfected with pFLAG-ATG7-VN, pVCn-HA-ATG12 and an individual cDNA expression vector encoding kinase and phosphatase protein in a mammalian expression vector for 24 h. Treatment of Amino acid starvation (EBSS) for 2 h or overexpression of pULK1 was used as positive control. Green fluorescence

images of the complementation were acquired under a fluorescence microscope (GFP channel).

Site-directed Mutagenesis

ZAK K45M mutant was generated by a Quikchange Site-Directed Mutagenesis kit (Stratagene) using synthetic oligonucleotides containing mutations in the corresponding positions. Mutation was verified by DNA sequencing analysis. The nucleotide changes in the mutant construct include: ZAK Lys45Met ($_{133}$AAG → $_{133}$ATG).

Antibodies and Western Blot Analysis

Cells were lyzed in ice-cold RIPA buffer (50 mM Tris-Cl pH 8.0, 15 mM NaCl, 1% Triton X-100, 0.5% sodium deoxycholate, 0.1% SDS, 1 mM PMSF, and 1 μg/ml each of aprotinin, leupeptin, and pepstatin A) and briefly sonicated. Cell lysates were clarified by centrifugation, resolved by SDS-PAGE, and proteins were transferred to PVDF using semidry blotter (Bio-Rad). The membrane was blocked with 3% BSA in TBS-T (10 mM Tris-Cl, pH 8.0, 150 mM NaCl, 0.05% Tween-20) and incubated overnight at 4 °C with primary antibodies. Immunoblots were visualized by enhanced

chemiluminescence method. The following antibodies were used for western blot analysis: LC3 (Novus), p62 (Abnova), actin, Tubulin, GFP, ZAK (Santa Cruz Biotechnology), and FLAG (Sigma).

Immunoprecipitation Assay

Cells were lyzed in RIPA buffer (50 mM Tris-Cl pH 7.5, 50 mM NaCl, 1% Triton X-100, 0.2% SDS, 1 mM EDTA, and 1 mM PMSF). After clarifying by centrifugation, cell lysates were incubated with anti-ZAK antibody or FLAG (M2) bead (Sigma) for 12 h at 4°C. After adding protein A/G-Bead (Santa Cruz Biotechnology), the mixtures were incubated for additional 6 h at 4°C. The immunocomplexes were washed five times with PBS, solubilized with sample buffer, and detected by western blotting as described above.

Immunostaining

Hep3B cells grown on coverslips in 24-well plates were co-transfected with pEGFP-ZAK and pFLAG-ATG7-VN for 24 h. Cells were then fixed with 4% paraformaldehyde for 15 min, permeabilized with 0.1% Triton X-100 for 1 min, and blocked with 3% BSA for 1 h. After stained with anti-FLAG (Sigma) for 12 h at 4 °C and Hoechst 33258, cells were visualized under a LSM

confocal fluorescence microscope (Zeiss). For mCherry-GFP-LC3 visualization, Hep3B cells were grown on coverslips in 24-well plates and co-transfected with pmCherry-GFP-LC3 and either pcDNA3-HA or pZAK for 24 h. Cells were then fixed with 4 % paraformaldehyde for 15 min, stained with Hoechst 33258 and visualized under a LSM confocal fluorescence microscope (Zeiss).

RT-PCR

Total RNA was purified from HEK293T, HeLa, MCF-7, and Hep3B cells using Trizol reagent and subjected to amplification with SuperScript One-Step RT–PCR system (Invitrogen). The following specific primers sets were used for PCR; *p62*, forward 5′-ATG GCC ATG TCC TAC GTG AAG GAT G-3′ and reverse 5′-AGA GGG CTA AGG GCA GCT GCC ACA C-3′; *ZAK*, forward 5′-ATG TCG TCT CTC GGT GCC TCC TTT G-3′ and reverse 5′-GAG GTC TCT GTG AAT CAC CTT GAC-3′; *β-actin*, forward 5′-GAG CTG CCT GAC GGC CAG G-3′ and reverse 5′-CAT CTG GAA GGT GGA C-3′.

Statistical Analysis

Differences between groups were analyzed using one-way analysis of variance (ANOVA) followed by Tukey's post-hoc test, or Student's *t*-test, as appropriate. Error bars represent S.D. or S.E.M., as indicated. $P < 0.05$ was considered statistically significant.

Results

Establishment of the ATG7-VN/VCn-ATG12 BiFC assay to screen autophagy modulators

ATG7 functions as an E1-like activating enzyme for ATG12, one of the substrates. ATG7 then transfers ATG12 to ATG5 through E2-like enzyme, ATG10 and the resulting ATG12-ATG5 conjugates sequentially interact with ATG16L1 that forms homodimer (Figure 1A). This ATG12-ATG5-ATG16L1 multimer complex functions as E3-like ligase for LC3-PE (phosphatidylethanolamine), resulting in the expansion of autophagosome. To identify novel autophagy modulator which regulates Ubiquitin-like (UBL) conjugation system, I established ATG7-VN/VCn-ATG12 bifluorescence complementation (BiFC) assay which allows the detection of the interaction between ATG7 and ATG12 with fluorescence complementation in living cells.

ATG7 was conjugated to the N-terminus of VENUS (VN173) to generate ATG7-VN. Because the C-terminus of ATG12 is modified for the conjugation**,** I conjugated VCn which is the C-terminus of VENUS (VC155) to the N-terminus of HA-ATG12 (Figure 1B). In this assay, it is important to note that monomeric form of ATG12 and ATG5 are present as well as ATG12-

ATG5 conjugated form. As expected, when cells were overexpressed with ATG5-HA, I could detect both monomeric ATG5 (~38 kDa) and conjugating form with endogenous ATG12 (~60 kDa) (Figure 1C). This result indicates that not only ATG12-ATG5 conjugated form but also monomeric form of ATG5 or ATG12 are expressed in mammalian cells.

ATG7-VN/VCn-ATG12 interaction is affected by autophagy signal

Using immunoprecipitation assay, I first confirmed the endogenous interaction between ATG7 and ATG12 in HEK293T cells (Figure 2A). Then I checked the ATG7-VN/VCn-ATG12 BiFC assay. Ectopic expression of ATG7-VN and VCn-ATG12 in HEK293T cells visualized GFP signal under a fluorescence microscope (Figure 2B). To further validate whether autophagy signals affect the intensity of BiFC fluorescence, both ATG7-VN and VCn-ATG12-transfected cells were exposed to amino acid starvation (EBSS) or co-expressed with ULK1. As a result, I observed that EBSS treatment or ULK1 expression enhanced the BiFC intensity (Figure 2B). In contrast, co-expression of mTOR, an autophagy repressor which inhibits ULK1, reduced the GFP-positive signal (Figure 2B).

Next, I addressed the direct interaction between ATG7-VN and VCn-ATG12. The results from immunoprecipitation assay revealed that ATG7-VN

binds to VCn-ATG12 in the transfected cells (Figure 2C). In addition, I found that the interaction between ATG7-VN and VCn-ATG12 increased under amino acid starvation (EBSS) compared to that of control cells. On the other hand, this interaction between ATG7-VN and VCn-ATG12 did not increase under amino acid starvation condition by the pre-treatment with 3-methyladenine (3-MA), a blocker of autophagosome formation (Figure 2C). As seen in the BiFC fluorescence, these results confirm that the interaction between ATG7 and ATG12 is regulated by autophagy signal.

Isolation of autophagy modulators affecting ATG7-VN/VCn-ATG12 BiFC

By utilizing the ATG7-VN/VCn-ATG12 BiFC assay, I performed gain-of-function screening to identify novel autophagy regulators. I screened 900 cDNAs in mammalian expression vector which encode kinase and phosphatase proteins in mammalian cells. After performing the primary screening of the cDNA library with the ATG7-VN/VCn-ATG12 BiFC assay in HEK293T cells, I isolated 22 putative positive clones which enhanced the BiFC intensity (Figure 3A). These putative positive clones were further assessed for their abilities to affect LC3-II conversion by secondary screening. To eliminate the possibility that the inhibition of autophagy also increases

LC3-II conversion, cells were treated Bafilomycin A1, a lysosomal inhibitor, to block lysosomal degradation. The results from western blotting showed that 9 clones among the 22 clones increased LC3-II conversion (Figure 3B).

Isolation of ZAK by ATG7-VN/VCn-ATG12 BiFC assay

Through the primary and secondary screenings, ZAK (sterile alpha motif and leucine zipper-containing kinase AZK) showed the most potent efficacy to induce autophagy among the putative positive clones. Therefore, I further investigated whether ZAK could regulate autophagy by affecting ATG7-ATG12 interaction. First, assessment with the ATG7-VN/VCn-ATG12 BiFC fluorescence assay revealed that overexpressed ZAK enhanced the fluorescence of ATG7-VN/VCn-ATG12 BiFC (Figure 4A). Second, co-immunoprecipitation assay followed by western blotting showed that ZAK significantly increased the interaction between ATG7-VN and VCn-ATG12 in the transfected cells (Figure 4B). These results suggest that ZAK might regulate the interaction between ATG7 and ATG12 to modulate autophagy machinery.

Depletion of ZAK increases the accumulation of p62

To determine the expressional levels of ZAK, RT-PCR analyses were performed in several cell lines. I found that ZAK was expressed in most of the cells with higher expression in Hep3B (Hepatocellular carcinoma) cells and MCF7 (Breast cancer) cells, and moderate level in HeLa (Cervical carcinoma) and HEK293T (Human embryonic kidney) cells (Figure 5A). Then I decided to knockdown ZAK expression with shRNA and assessed autophagy in the cells. Unfortunately, due to the limitation of antibody against ZAK, it was rare to detect endogenous levels of ZAK expression. Instead, I examined knockdown effects of ZAK shRNAs in HEK293T cells overexpressing exogenous ZAK.

Western blot analysis revealed that ZAK shRNA#1 was marginal to reduce the level of overexpressed ZAK, while ZAK shRAN#2 was better and almost reduced ZAK expression (Figure 5B). Similarly, RT-PCR analysis revealed that ZAK shRAN#2 efficiently reduced the level of endogenous ZAK mRNA in HEK293T cells (Figure 5D). Then, I examined the degradation of autophagy substrate p62 in Hep3B cells. Immunocytochemical analysis revealed that compared to control cells, transfection with ZAK shRNA #2 increased the level of endogenous p62 in Hep3B cells (Figure 5C). Accordingly, knockdown of ZAK expression accumulated the levels of p62, consistent with the results of immunocytochemistry (Figure 5D). These results indicate that ZAK activates the basal level of autophagy.

ZAK is essential for starvation-induced autophagy and oxidative stress-induced autophagy

Since the functional role of ATG7 has been revealed in common autophagy machinery, ZAK was further investigated for its effect on starvation-induced autophagy. Under serum starvation, down regulation of ZAK inhibited both LC3-II conversion and GFP-LC3 puncta formation (Figure 6A and B). Further, under amino acid starvation (EBSS), knockdown of ZAK expression blocked the formation of GFP-LC3 puncta. Moreover, when Hep3B cells expressing GFP-LC3 were incubated with hydrogen peroxide (H_2O_2), the increased number of GFP-LC3 puncta was abolished in ZAK depleted cells. These results demonstrate that ZAK plays an essential role in both starvation-induced autophagy and oxidative stress-induced autophagy.

Ectopic expression of ZAK increases autophagy flux

Conversely, western blot analysis showed that overexpression of ZAK increased LC3-II conversion and this increment was further accomplished by Bafilomycin A1 treatment (Figure 7A), meaning that the increase of LC3-II is not due to the inhibition of autophagy flux. Accordingly,

overexpression of ZAK reduced p62 level in the cells. Consistently, the formation of GFP-LC3 puncta was increased by ZAK overexpression and this increase was blocked by the treatment with 3-methyladenine (3-MA), a class III PI3K inhibitor (Figure 7B). In addition, I measured autophagy flux using tandem mCherry-GFP-LC3 assay in which GFP is labile in acidic condition and the fluorescence therefore is lost in the lysosome, while mCherry is not. I discriminated the autophagosomes (GFP/RFP positive) from autolysosomes (RFP only signal). The results showed that overexpression of ZAK increased not only total number of LC3 puncta but also RFP only autolysosomes dramatically (Figure 7C). These observations indicate that overexpression of ZAK increases autophagy flux.

Kinase activity of ZAK is required for the regulation of autophagy

Because ZAK is a serine/threonine kinase, cells were further investigated whether the kinase activity of ZAK is essential for its effect. By immunoprecipitation assay, phosphorylated ZAK was detected, assuming kinase activity of ZAK might function to regulate autophagy (Figure 8A). According to the previous report (Wang et al., 2014), lysine 45 of ZAK is essential for it kinase activity. Thus I generated a kinase-dead mutant (ZAK K45M) with site-directed mutagenesis. Unlike wild-type ZAK,

overexpression of ZAK K45M did not reduce the levels of p62 and ubiquitin-conjugates but rather increased those (Figure 8B). Similarly, overexpression of ZAK K45M did not enhance the formation of GFP-LC3 puncta (Figure 8C), indicating that autophagy-stimulating activity of ZAK requires the kinase activity.

The effect of ZAK K45M was further confirmed on starvation-induced autophagy. Under amino acid starvation, I found that overexpression of ZAK potentiated amino acid starvation-induced autophagy (Figure 8C). Interestingly, overexpression of ZAK K45M suppressed amino acid starvation-induced GFP-LC3 puncta formation. Compared to GFP-LC3 puncta formation (22%) in control cells, it was further reduced to 8% in ZAK K45M-transfected cells under amino acid-starvation condition (Figure 8C). These results indicate that ZAK K45M may act as a dominant negative mutant during amino acid- starvation condition.

ZAK interacts with ATG7

The observation that ZAK K45M may act as a dominant negative mutant led me to address whether ZAK binds to ATG7 or ATG12. Therefore, the interaction between ZAK and ATG7 was investigated in the cells. The results from immunoprecipitation assay revealed that ZAK bound to ATG7-

FLAG in the transfected cells (Figure 9A and B). Immunocytochemistry assay also showed that GFP-ZAK co-localized with FLAG-ATG7 in the transfected Hep3B cells (Figure 9C). However, ZAK did not interact with ATG12 (data not shown). Unfortunately, there are no available antibodies against endogenous ZAK and ATG7 for immunocytochemical analysis. These results suggest that ZAK regulates autophagy through its interaction with ATG7, possibly by phosphorylating ATG7.

Figure II-1. Establishment of the ATG7-VN/VCn-ATG12 BiFC assay to screen autophagy modulators. (A) ATG12-ATG5 conjugation system in mammalian cells. (B) Schematic diagram showing ATG7-VN/VCn-ATG12 BiFC assay. (C) Monomeric and conjugated forms of ATG5 in mammalian cells. HEK293T cells were transfected with ATG5-HA for 24 h. Cells were then harvested and subjected to western blot analysis using anti-HA antibody.

Figure II-1

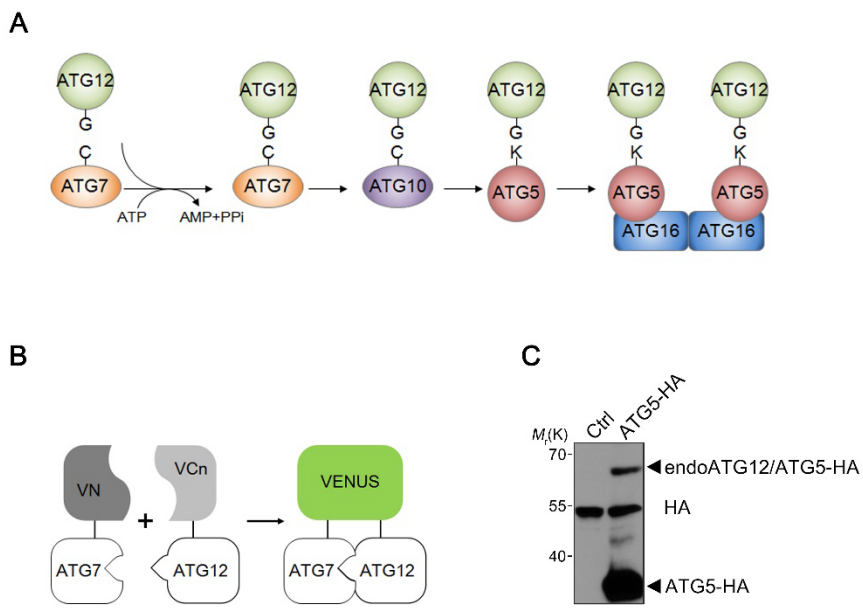
A
ATG12
G
C
ATG7
ATP
AMP+PPi
ATG12
G
C
ATG7
ATG12
G
C
ATG10
ATG12
G
K
ATG5
ATG12
G
K
ATG5
ATG16
ATG12
G
K
ATG5
ATG16
B
VN
VCn
VENUS
ATG7
ATG12
ATG7
ATG12
C
Ctrl
ATG5-HA
M_r(K)
70-
55-
40-
endoATG12/ATG5-HA
HA
ATG5-HA

Figure II-2. Interaction between ATG7-VN and VCn-ATG12 is modulated by autophagy signal. (A) Endogenous interaction between ATG7 and ATG12. HEK293T cell extracts were subjected to immunoprecipitation (IP) assay using anti-ATG7 antibody. The immunoprecipitates and whole cell lysates (WCL) were analyzed by western blotting. (B) Visualization of ATG7-VN/VCn-ATG12 association in living cells. HEK293T cells were co-transfected with pVCn-HA-ATG12, pFLAG-ATG7-VN and either pcDNA3 (Ctrl, EBSS), pULK1 or pmTOR for 19 h and then incubated with serum-supplemented full media (Ctrl, ULK1, mTOR) or amino acid-free media (EBSS) for additional 3 h. Green fluorescence images of the complementation were acquired under a fluorescence microscope (GFP channel). (C) Interaction between ATG7-VN and VCn-ATG12 is regulated by autophagy signal. HEK293T cells were co-transfected with pVCn-HA-ATG12 and pFLAG-ATG7-VN for 19 h. Cells were then cultured with either full media or EBSS for additional 2 h or with full media containing 5 mM 3-MA for 6 h. Cell extracts were subjected to immunoprecipitation (IP) assay with anti-HA antibody. The immunoprecipitates and whole cell lysates (WCL) were analyzed by western blotting.

Figure II-2

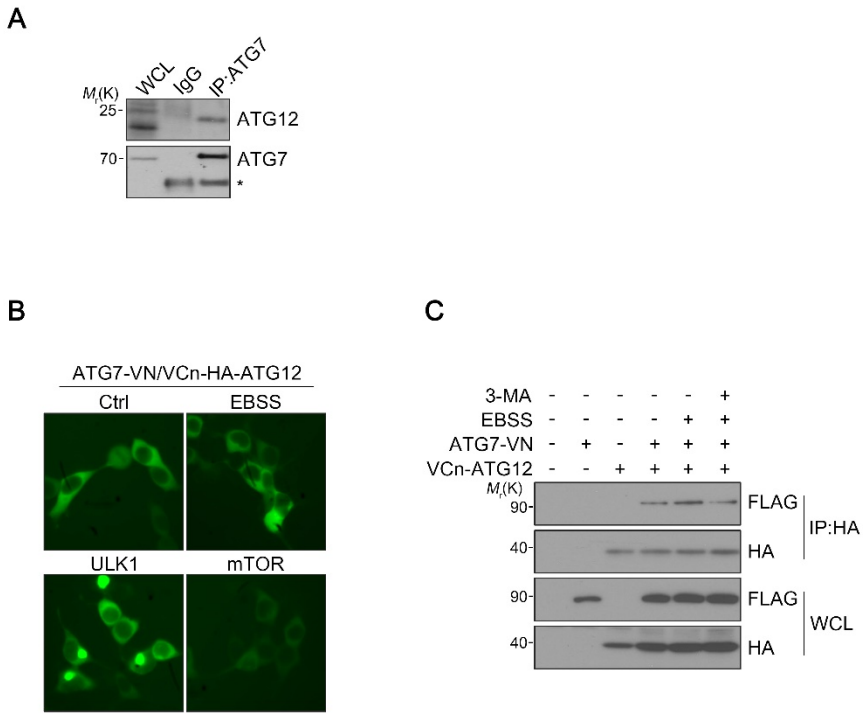
A
WCL
IgG
IP:ATG7
M_r(K)
25-
ATG12
70-
ATG7
*
B
ATG7-VN/VCn-HA-ATG12
Ctrl
EBSS
ULK1
mTOR
C
3-MA - - - - - +
EBSS - - - - + +
ATG7-VN - + - + + +
VCn-ATG12 - - + + + +
M_r(K)
90-
FLAG
IP:HA
40-
HA
90-
FLAG
WCL
40-
HA

Figure II-3. Isolation of the putative positive clones using ATG7-VN/VCn-ATG12 BiFC assay. (A) Selection of putative positive clones enhancing ATG7-VN/VCn-ATG12 BiFC signal. HEK293T cells were co-transfected with pVCn-HA-ATG12, pFLAG-ATG7-VN and each of mammalian expression cDNA Library for 24 h. Green fluorescence images of the complementation were acquired under a fluorescence microscope (GFP channel). Amino acid starvation (EBSS) and overexpression of ULK were used as positive controls. (B) Overexpression effects of the putative positive clones on LC3-II conversion. HEK293T cells were transfected with the each putative positive clones for 24 h and then treated with 10 nM Bafilomycin A1 (Baf. A1) for additional 2 h. Cells were harvested and subjected to western blot analysis.

Figure II-3

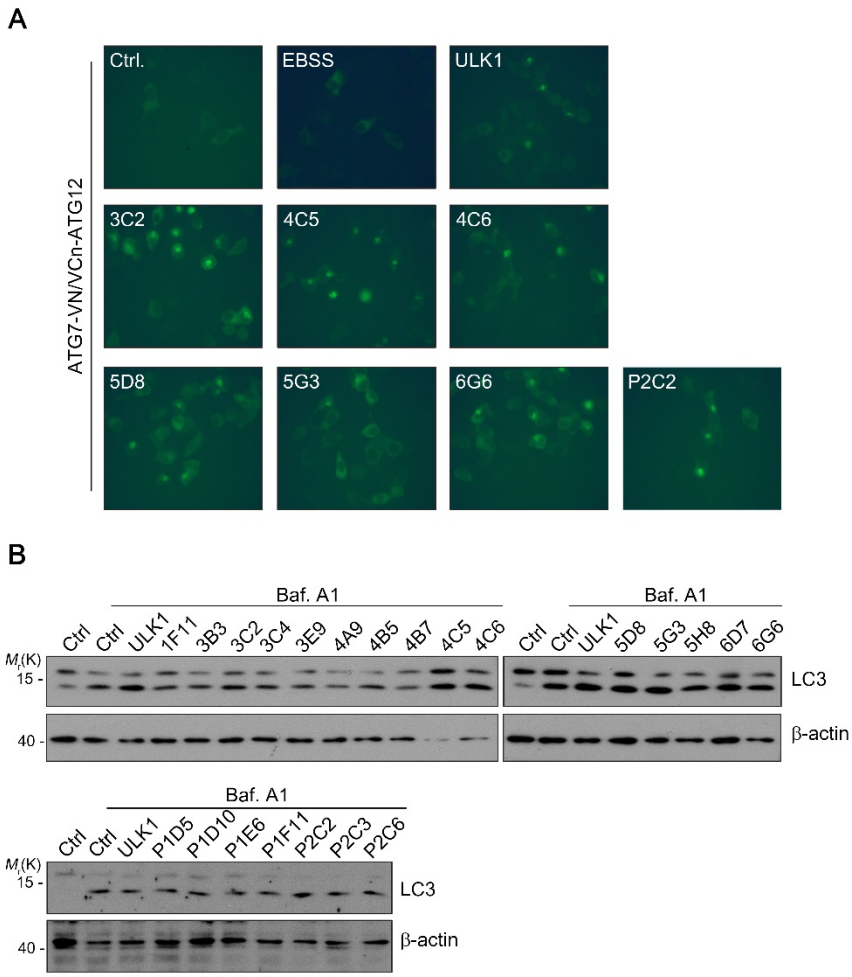
A
ATG7-VN/VCn-ATG12
Ctrl.
EBSS
ULK1
3C2
4C5
4C6
5D8
5G3
6G6
P2C2
B
Baf. A1
Ctrl
Ctrl
ULK1
1F11
3B3
3C2
3C4
3E9
4A9
4B5
4B7
4C5
4C6
Baf. A1
Ctrl
Ctrl
ULK1
5D8
5G3
5H8
6D7
6G6
M_r(K)
15 -
40 -
LC3
β-actin
Baf. A1
Ctrl
Ctrl
ULK1
P1D5
P1D10
P1E6
P1F11
P2C2
P2C3
P2C6
M_r(K)
15 -
40 -
LC3
β-actin

Figure II-4. ZAK increases ATG7-VN/VCn-ATG12 BiFC signal and interaction between them. (A) Enhanced BiFC signals of ATG7-VN/VCn-ATG12 by ZAK overexpression. HEK293T cells were co-transfected with pVCn-HA-ATG12, pFLAG-ATG7-VN, and either pcDNA3-HA (Ctrl) or pZAK for 24 h. Green fluorescence images of the complementation were acquired under a fluorescence microscope (GFP channel). (B) Enhanced binding between ATG7-VN and VCn-ATG12 by ZAK overexpression. After transfection with pVCn-HA-ATG12, pFLAG-ATG7-VN, and either pcDNA3-HA or pZAK for 24 h, HEK293T cell extracts were analyzed with immunoprecipitation (IP) assay using anti-FLAG (M2) antibody. The immunoprecipitates and whole cell lysates (WCL) were analyzed by western blot analysis.

Figure II-4

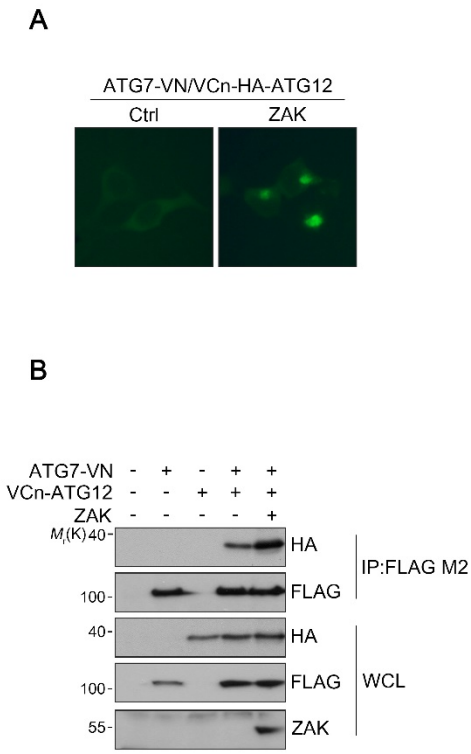
A
ATG7-VN/VCn-HA-ATG12
Ctrl
ZAK
B
ATG7-VN - + - + +
VCn-ATG12 - - + + +
ZAK - - - - +
M_r(K) 40-
HA
IP:FLAG M2
100-
FLAG
40-
HA
WCL
100-
FLAG
55-
ZAK

Figure II-5. Depletion of ZAK expression increases p62 accumulation. (A) RT-PCR analysis showing ZAK mRNA level in cell lines. Total RNA was purified from HEK293T, HeLa, MCF7, and Hep3B cells and analyzed by reverse transcriptase-polymerase chain reaction (RT-PCR) using gene-specific synthetic primers. (B) Effect of ZAK shRNA on ZAK expression. HEK293T cells were co-transfected with pZAK and either pZAK shRNA#1 or #2 for 48 h. Cells were harvested and subjected to western blot analysis using anti-ZAK antibody. (C) ZAK shRNA#2 accumulates p62 aggregates. Hep3B cells grown on coverslip were transfected with pSuper-neo (Control, Ctrl), pZAK shRNA #1, or pZAK shRNA #2 for 48 h. Cells were then fixed with 4% paraformaldehyde, permeabilized with 0.1% Triton X-100, blocked with 3% BSA, and incubated with anti-p62 antibody for 12 h at 4℃. (D) Effect of ZAK shRNA on ZAK mRNA level and autophagy. HEK293T cells were transfected with pSuper-neo, pZAK shRNA #1, or pZAK shRNA #2 for 48 h. Cells were harvested for either western blot analysis (*upper*) or RT-PCR (*lower*). Total RNA was purified and analyzed by RT-PCR using gene-specific synthetic primers.

Figure II-5

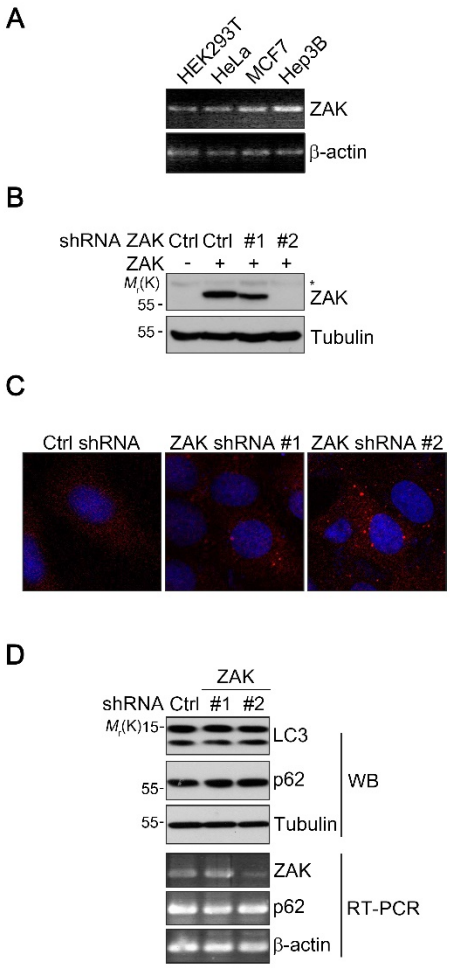
A
HEK293T
HeLa
MCF7
Hep3B
ZAK
β-actin
B
shRNA ZAK Ctrl Ctrl #1 #2
ZAK - + + +
Mr(K)
55-
ZAK
55-
Tubulin
C
Ctrl shRNA
ZAK shRNA #1
ZAK shRNA #2
D
ZAK
shRNA Ctrl #1 #2
Mr(K)15-
LC3
55-
p62
WB
55-
Tubulin
ZAK
p62
RT-PCR
β-actin

Figure II-6. Knockdown of ZAK inhibits starvation-induced autophagy and oxidative stress-induced autophagy. (A and B) Knockdown of ZAK expression inhibits serum starvation-induced autophagy. Hep3B cells were co-transfected with pEGFP-LC3 and either pSuper-neo, pZAK shRNA #1, or pZAK shRNA #2 for 48 h. Cells were further incubated with either full medium or serum-starved medium for 3 h. Cells showing GFP-LC3 puncta were counted under a fluorescence microscope (A). HEK293T cells were transfected with either pSuper-neo, pZAK shRNA #2, or pZAK shRNA #2 for 24 h. Cells were then either exposed to full medium or serum-starved medium for 3 h and harvested for western blot analysis (B). Bars represent mean values ± S.D. (n > 3). (C) Knockdown of ZAK expression inhibits amino acid starvation-induced autophagy. Hep3B cells were co-transfected with pEGFP-LC3 and either pSuper-neo, pZAK shRNA #1, or pZAK shRNA #2 for 48 h and further incubated with either full medium or EBSS for 2 h. Cells showing GFP-LC3 puncta were counted under a fluorescence microscope. (D) Knockdown of ZAK expression inhibits autophagy in response to H_2O_2. Hep3B cells were co-transfected with pEGFP-LC3 and either pSuper-neo, pZAK shRNA #1, or pZAK shRNA #2 for 48 h, and the cells were left untreated (Veh) or treated with 0.5 mM H_2O_2 for additional 3 h. Cells showing GFP-LC3 puncta were counted under a fluorescence microscope. * P < 0.05, ** P < 0.01, *** P < 0.001.

Figure II-6

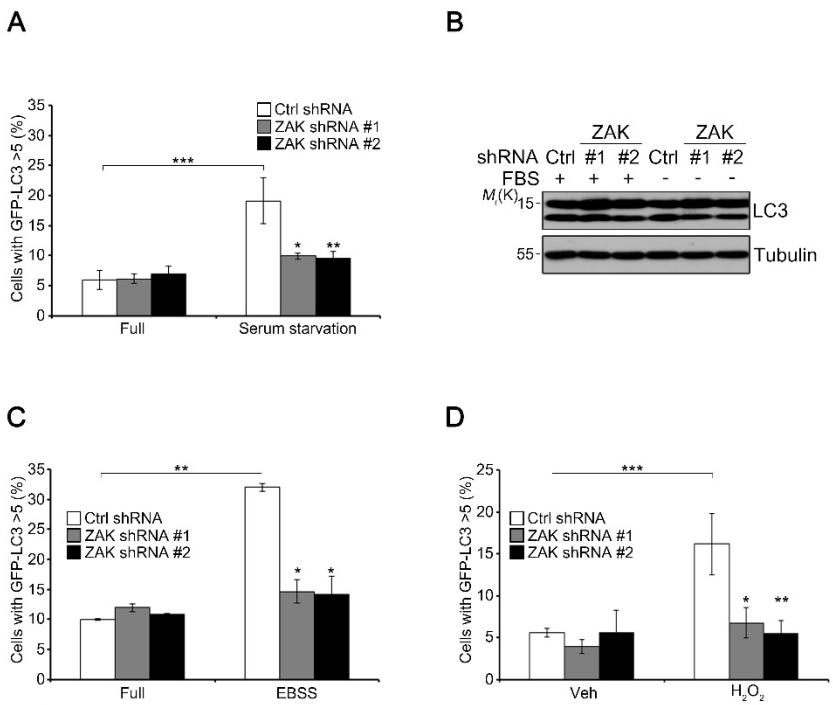
A
B
C
D
Ctrl shRNA
ZAK shRNA #1
ZAK shRNA #2
Cells with GFP-LC3 >5 (%)
Full
Serum starvation
EBSS
Veh
H_2O_2
shRNA Ctrl #1 #2 Ctrl #1 #2
ZAK
ZAK
FBS + + + - - -
M_r(K)
15-
55-
LC3
Tubulin

Figure II-7. Ectopic expression of ZAK increases autophagy flux. (A) Overexpression of ZAK increases LC3-II conversion. HEK293T cells were transfected with either pcDNA3-HA or pZAK for 24 h in the absence or presence of 20 nM Bafilomycin A1. Cells were harvested for western blot analysis using the indicated antibodies. (B) Autophagy inhibitor 3-MA blocks ZAK-induced increase of GFP-LC3 dots. Hep3B cells were co-transfected with pEGFP-LC3 and either pcDNA3-HA or pZAK for 24 h and treated with 5 mM 3-MA cells for 6 h before cells were harvested. Cells showing GFP-LC3 puncta were counted under a fluorescence microscope. Bars represent mean values ± S.D. (n > 3). (C) Increase of autophagic flux by ZAK expression. Hep3B cells grown on coverslips were co-transfected with pmCherry-GFP-LC3 and either pcDNA3-HA or pZAK for 24 h. After fixing the cells with 4% paraformaldehyde, GFP green (*upper*) and mCherry red (*middle*) fluorescence images were acquired under a confocal microscope. The number of LC3 puncta showing GFP^+/RFP^+ or GFP^-/RFP^+ were counted and represented with bars (*right*) (mean values ± S.E.M., n = 21). ** $P < 0.01$, *** $P < 0.001$.

Figure II-7

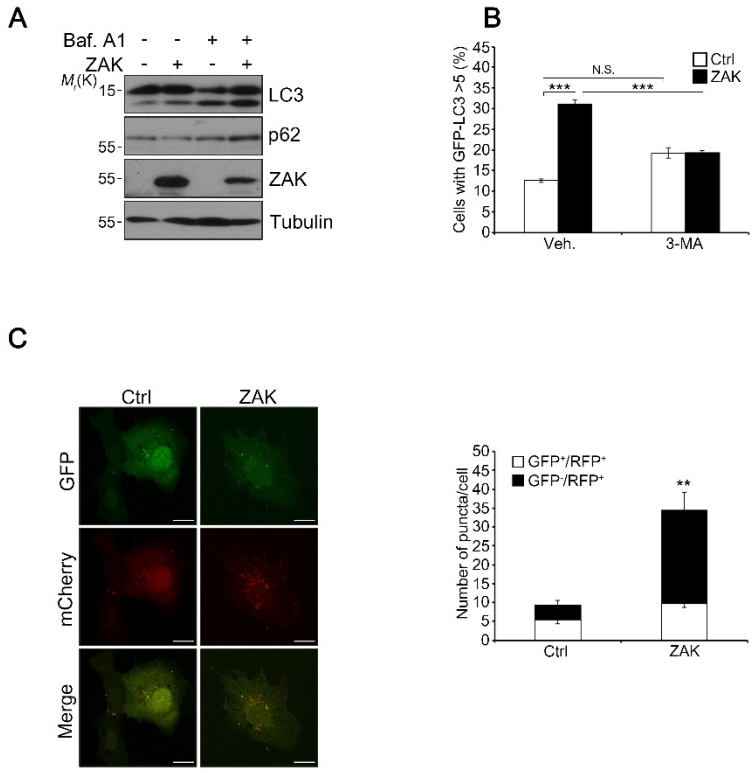
A
Baf. A1 - - + +
ZAK - + - +
M_r(K)
15-
LC3
55-
p62
55-
ZAK
55-
Tubulin
B
Cells with GFP-LC3 >5 (%)
N.S.
***
***
Ctrl
ZAK
Veh.
3-MA
C
Ctrl
ZAK
GFP
mCherry
Merge
Number of puncta/cell
GFP+/RFP+
GFP-/RFP+
**
Ctrl
ZAK

Figure II-8. Kinase activity of ZAK regulates autophagy. (A) Kinase activity of ZAK. HEK293T cells were transfected either pcDNA3-HA or pZAK for 24 h. Cell extracts were analyzed with immunoprecipitation (IP) assay using anti-phospho-Serine antibody. The immunoprecipitates and whole cell lysates (WCL) were analyzed by western blot analysis. (B and C) Kinase activity of ZAK is required for autophagy activation. HEK293T cells were transfected with either pcDNA3-HA, pZAK, or pZAK K45M for 24 h. Cells were then harvested for western blot analysis (B). Hep3B cells were co-transfected with pEGFP-LC3 and either pcDNA3-HA, pZAK, or pZAK K45M for 24 h. Cells showing GFP-LC3 were counted under a fluorescence microscope (C). (D) Kinase activity of ZAK is required for amino acid starvation-induced autophagy. Hep3B cells were co-transfected with pEGFP-LC3 and either pcDNA3-HA, pZAK, or pZAK K45M for 24 h. Cells were then incubated with either full medium or amino acid-free medium (EBSS) for 2 h. Cells showing GFP-LC3 were counted under a fluorescence microscope. Bars represent mean values ± S.D. ($n > 3$). ** $P < 0.01$, *** $P < 0.001$.

Figure II-8

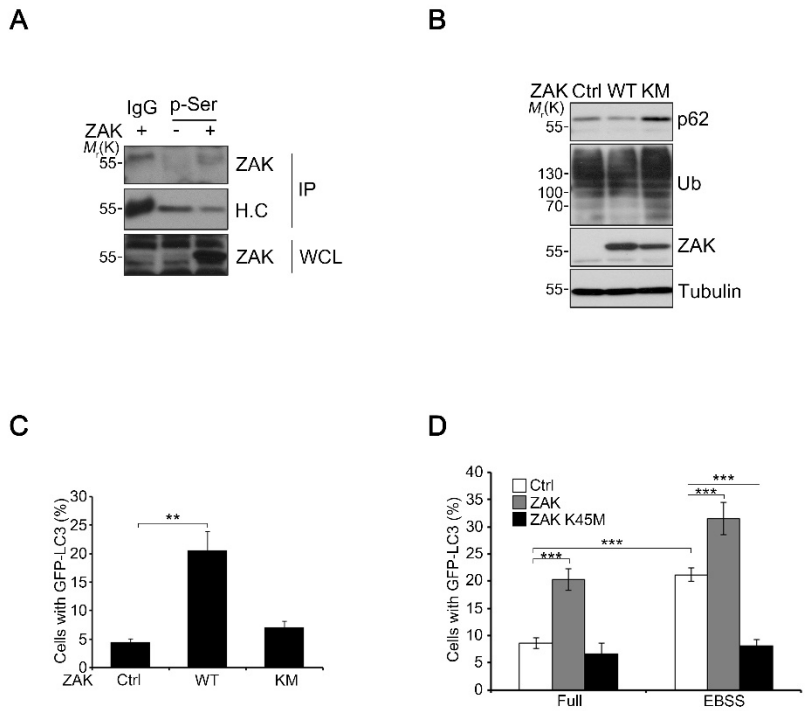
A
IgG
p-Ser
ZAK + - +
M_r(K)
55-
ZAK
IP
55-
H.C
55-
ZAK
WCL
B
ZAK Ctrl WT KM
M_r(K)
55-
p62
130-
100-
70-
Ub
55-
ZAK
55-
Tubulin
C
Cells with GFP-LC3 (%)
30
25
20
15
10
5
0
**
ZAK Ctrl WT KM
D
Cells with GFP-LC3 (%)
40
35
30
25
20
15
10
5
0
Ctrl
ZAK
ZAK K45M
***
***
***
***
Full
EBSS

Figure II-9. ZAK interacts and colocalizes with ATG7. (A and B) ZAK interacts with ATG7. HEK293T cells were transfected with pFLAG-ATG7-VN and pZAK for 24 h. Cells were then subjected to immunoprecipitation (IP) assay with anti-FLAG (M2) (A) or anti-ZAK antibody (B). The immunoprecipitates and whole cell lysates (WCL) were analyzed by western blotting. (C) ATG7 co-localizes with ZAK. Hep3B cells grown on coverslip were co-transfected with pEGFP-ZAK and pFLAG-ATG7-VN for 24 h. Cells were then fixed with 4% paraformaldehyde, permeabilized with 0.1% Triton X-100, blocked with 3% BSA, and immunostained with anti-FLAG antibody for 12 h at 4℃. Fluorescence images were acquired under a confocal microscope

Figure II-9

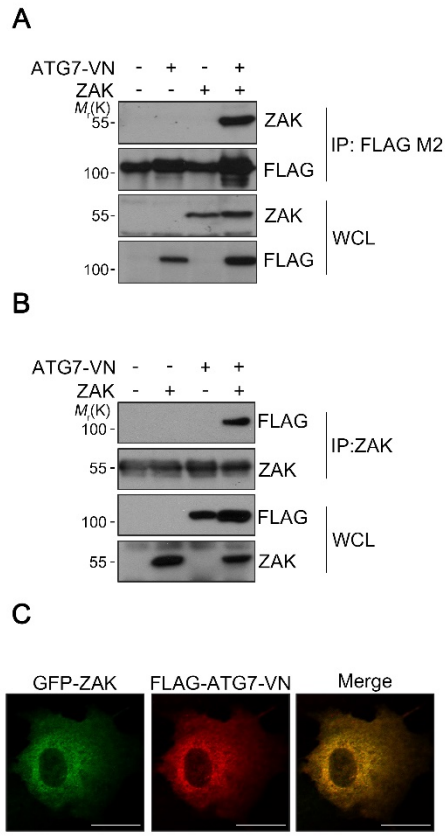
A
ATG7-VN - + - +
ZAK - - + +
M_r(K)
55-
ZAK
IP: FLAG M2
100-
FLAG
55-
ZAK
WCL
100-
FLAG
B
ATG7-VN - - + +
ZAK - + - +
M_r(K)
100-
FLAG
IP:ZAK
55-
ZAK
100-
FLAG
WCL
55-
ZAK
C
GFP-ZAK
FLAG-ATG7-VN
Merge

Figure II-10. Schematic diagram of ZAK-mediated autophagy as an ATG7 regulator. Under various autophagy stimulation signals, ZAK phosphorylates ATG7 to strengthen the interaction with ATG12, thereby enhances autophagy flux.

Figure II-10

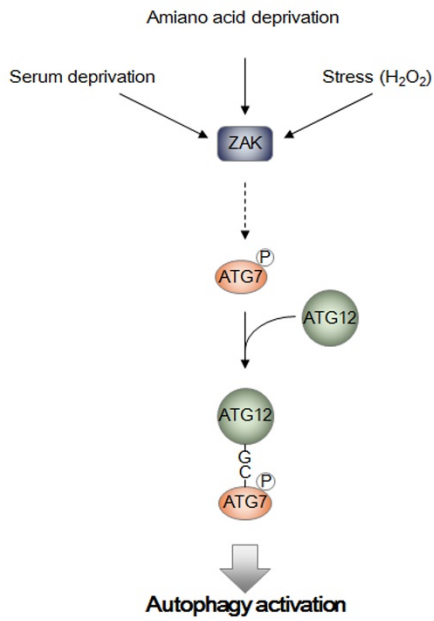
Amiano acid deprivation
Serum deprivation
Stress (H_2O_2)
ZAK
ATG7
P
ATG12
ATG12
G
C
P
ATG7
Autophagy activation

Discussion

Studies on autophagy machinery revealed various ATG proteins and their concerted action to form auotphagosome. However, the precise mechanism for its upstream signaling and post-translational modifications of ATGs is not fully understood. Especially the activity and regulation of ATG7 is not known. ATG7 is an E1-like enzyme and plays an important role in both ATG12-5 and LC3-PE conjugation. Unlike LC3-PE conjugates, it has been thought that ATG12-ATG5 conjugates are irreversible process. Moreover, it is still controversial whether unconjugated forms of ATG12 and ATG5 are detectable or not (Mizushima et al., 2001; Thompson et al., 2005). I observed that overexpressed ATG5 forms conjugation with endogenous ATG12 and is also present as a monomeric form. Because ATG7 acts like E1 enzyme to modulate two UBL conjugation systems that function to elongate the phagophore, it is important to understand the regulatory mechanism of ATG7 modulation during autophagy.

To isolate novel regulators autophagy, ATG7-VN/VCn-ATG12 BiFC assay was adopted. This assay is based on the interaction of ATG7-12 in the cells, as we also observed. Actually I also tried to establish ATG5-VN/VCn-

ATG12 BiFC assay but could not observe any difference in the intensity of the fluorescence during autophagy (data not shown). In contrast, the intensity in the fluorescence of ATG7-VN/VCn-ATG12 BiFC assay reflects with the levels of autophagy activity. Thus, I employed this assay for the screening and identified ZAK as a most potent autophagy regulator. To my surprise, down-regulation of ZAK inhibited starvation-induced autophagy. For this activity, the kinase activity is essential. From this point of view, I conclude that the kinase activity of ZAK is indispensable for its regulation role in autophagy. Moreover, the observation that ZAK interacted with ATG7 further implies an autophagy regulatory role of ZAK by phosphorylating ATG7, which remains to be further addressed performed. It also remains to be investigated which domain of ZAK is required for ATG7-ZAK interaction and which Ser/Thr residues of ATG7 are modified by ZAK. Recently, constitutive (S230E, S234E) active forms of ZAK have reported to activate JNK and NF-κB signaling pathway mimicking the extracellular stimuli. It will be interesting to test whether kinase activity of ZAK is essential to ATG7 for autophagy regulation using constitutively active form of ZAK.

To adapt to the rapid alteration of environmental stress, cells utilize post-translational modification (PTM) to transit protein activity. Until now, a numbers of reports showed post-translational modifications of ATGs for autophagy regulation; phosphorylation, acetylation, and ubiquitination (Feng

et al., 2015). An E3 ubiquitin ligase, TRAF6 (TNF receptor-associated factor 6) reported to ubiquitinate Beclin1 and ULK1 (Nazio et al., 2013; Shi and Kehrl, 2010). The Lys63 (K63)-linked ubiquitination of Beclin1 and ULK1 leads to induction of autophagy. In addition, RNF5 (ring finger protein 5) ubiquitinates ATG4B to facilitate its degradation for autophagy inhibition. Acetylation is well-known to play a key role in the regulation of ATGs gene transcription. ULK1 is directly acetylated by KAT5/TIP60 and the modification results in autophagy initiation (Lin et al., 2012). Esa1, a yeast ortholog of KAT5 [K (lysine) acetyltransferase 5], is a diseases-associated gene, including HIV-1 and Kaposi's sarcoma. Esa1 acetylates Atg3 and accelerates Atg8-Atg3 interaction (Yi et al., 2012). Several major ATG proteins, including ATG5, ATG7, ATG12, and LC3 also experienced an acetylation via EP300/p300 (E1A binding protein p300) acetyltransferase, reducing their functions. Conversely, SIRT1 deacetylates ATG5, ATG7, and LC3 to enhance autophagosome formation. Acetylation also regulates FOXO3, a transcription factor, and the acetylated FOXO3 is interacted with an E1-like protein ATG7 to modulate autophagy by modulating protein–protein interactions. (Attaix and Bechet, 2007; Zhao et al., 2007). Phosphorylation is the last form of PTM. To date, ULK1 is the only kinase whose kinase activity is modulated by phosphorylation among ATGs. mTORC1 and AMPK are the well-known upstream kinases for ULK1

phosphorylation to regulate autophagy initiation step (Jung et al., 2010; Kim et al., 2011). Phosphorylated Beclin1 by DAPK (death-associated protein kinase) disrupts the interaction between Beclin1 and Bcl-XL, therefore allowing beclin1 to associate with class III PI3K to activate autophagy (Zalckvar et al., 2009). More elucidation for the modification of autophagy machinery allows cells to adapt with distinct environments through autophagy.

In addition to the function of ZAK in ATG7-ATG12 pathway, the role of ZAK as an E1-like enzyme for LC3-PE conjugate (Ichimura et al., 2000) remains to be further elucidated. In addition two isoforms of ZAK, ZAK-α (91 kDa) and ZAK-β (51 kDa), which are generated by alternative transcription (Gotoh et al., 2001) and have identical kinase domains, including the ATP binding site, need to be compared for their activity in the regulation of autophagy. Especially, ZAK-α, the longer form, contains SAM domain and thus the effect of ZAK-α on autophagy regulation and phosphorylation of ATG proteins should be defined. Further, characterization on upstream and downstream signaling of ZAK are needed for both ZAK-α and ZAK-β. In conclusion, this study first demonstrates a post-translational modification of ATG7 by ZAK which is now essential component in autophagy activation.

References

Attaix, D., and Bechet, D. (2007). FoxO3 controls dangerous proteolytic liaisons. Cell metabolism *6*, 425-427.

Chen, D., Zhu, C., Wang, X., Feng, X., Pang, S., Huang, W., Hawley, R.G., and Yan, B. (2013). A novel and functional variant within the ATG5 gene promoter in sporadic Parkinson's disease. Neurosci Lett *538*, 49-53.

Cuervo, A.M., and Dice, J.F. (1996). A receptor for the selective uptake and degradation of proteins by lysosomes. Science *273*, 501-503.

Dunn, W.A., Jr., Cregg, J.M., Kiel, J.A., van der Klei, I.J., Oku, M., Sakai, Y., Sibirny, A.A., Stasyk, O.V., and Veenhuis, M. (2005). Pexophagy: the selective autophagy of peroxisomes. Autophagy *1*, 75-83.

Feng, Y., He, D., Yao, Z., and Klionsky, D.J. (2014). The machinery of macroautophagy. Cell research *24*, 24-41.

Feng, Y., Yao, Z., and Klionsky, D.J. (2015). How to control self-digestion: transcriptional, post-transcriptional, and post-translational regulation of autophagy. Trends Cell Biol *25*, 354-363.

Fujita, N., Itoh, T., Omori, H., Fukuda, M., Noda, T., and Yoshimori, T. (2008). The Atg16L complex specifies the site of LC3 lipidation for membrane biogenesis in autophagy. Molecular biology of the cell *19*, 2092-2100.

Gallo, K.A., and Johnson, G.L. (2002). Mixed-lineage kinase control of JNK and p38 MAPK pathways. Nature reviews Molecular cell biology *3*, 663-672.

Geng, J., and Klionsky, D.J. (2008). The Atg8 and Atg12 ubiquitin-like conjugation systems in macroautophagy. 'Protein modifications: beyond the usual suspects' review series. EMBO reports *9*, 859-864.

Gotoh, I., Adachi, M., and Nishida, E. (2001). Identification and characterization of a novel MAP kinase kinase kinase, MLTK. The Journal of biological chemistry *276*, 4276-4286.

Gross, E.A., Callow, M.G., Waldbaum, L., Thomas, S., and Ruggieri, R. (2002). MRK, a mixed lineage kinase-related molecule that plays a role in gamma-radiation-induced cell cycle arrest. The Journal of biological chemistry *277*, 13873-13882.

Hampe, J., Franke, A., Rosenstiel, P., Till, A., Teuber, M., Huse, K., Albrecht, M., Mayr, G., De La Vega, F.M., Briggs, J., *et al.* (2007). A genome-wide association scan of nonsynonymous SNPs identifies a susceptibility variant for Crohn disease in ATG16L1. Nat Genet *39*, 207-211.

Hong, S.B., Kim, B.W., Lee, K.E., Kim, S.W., Jeon, H., Kim, J., and Song, H.K. (2011). Insights into noncanonical E1 enzyme activation from the structure of autophagic E1 Atg7 with Atg8. Nat Struct Mol Biol *18*, 1323-1330.

Hwang, S., Maloney, N.S., Bruinsma, M.W., Goel, G., Duan, E., Zhang, L.,

Shrestha, B., Diamond, M.S., Dani, A., Sosnovtsev, S.V., *et al.* (2012). Nondegradative role of Atg5-Atg12/ Atg16L1 autophagy protein complex in antiviral activity of interferon gamma. Cell Host Microbe *11*, 397-409.

Ichimura, Y., Kirisako, T., Takao, T., Satomi, Y., Shimonishi, Y., Ishihara, N., Mizushima, N., Tanida, I., Kominami, E., Ohsumi, M., *et al.* (2000). A ubiquitin-like system mediates protein lipidation. Nature *408*, 488-492.

Jung, C.H., Ro, S.H., Cao, J., Otto, N.M., and Kim, D.H. (2010). mTOR regulation of autophagy. FEBS letters *584*, 1287-1295.

Kaiser, S.E., Mao, K., Taherbhoy, A.M., Yu, S., Olszewski, J.L., Duda, D.M., Kurinov, I., Deng, A., Fenn, T.D., Klionsky, D.J., *et al.* (2012). Noncanonical E2 recruitment by the autophagy E1 revealed by Atg7-Atg3 and Atg7-Atg10 structures. Nat Struct Mol Biol *19*, 1242-1249.

Kim, I., Rodriguez-Enriquez, S., and Lemasters, J.J. (2007). Selective degradation of mitochondria by mitophagy. Archives of biochemistry and biophysics *462*, 245-253.

Kim, J., Kundu, M., Viollet, B., and Guan, K.L. (2011). AMPK and mTOR regulate autophagy through direct phosphorylation of Ulk1. Nature cell biology *13*, 132-141.

Komatsu, M., Tanida, I., Ueno, T., Ohsumi, M., Ohsumi, Y., and Kominami, E. (2001). The C-terminal region of an Apg7p/Cvt2p is required for homodimerization and is essential for its E1 activity and E1-E2 complex

formation. The Journal of biological chemistry *276*, 9846-9854.

Komatsu, M., Waguri, S., Ueno, T., Iwata, J., Murata, S., Tanida, I., Ezaki, J., Mizushima, N., Ohsumi, Y., Uchiyama, Y., *et al.* (2005). Impairment of starvation-induced and constitutive autophagy in Atg7-deficient mice. J Cell Biol *169*, 425-434.

Korkina, O., Dong, Z., Marullo, A., Warshaw, G., Symons, M., and Ruggieri, R. (2013). The MLK-related kinase (MRK) is a novel RhoC effector that mediates lysophosphatidic acid (LPA)-stimulated tumor cell invasion. The Journal of biological chemistry *288*, 5364-5373.

Kuma, A., Hatano, M., Matsui, M., Yamamoto, A., Nakaya, H., Yoshimori, T., Ohsumi, Y., Tokuhisa, T., and Mizushima, N. (2004). The role of autophagy during the early neonatal starvation period. Nature *432*, 1032-1036.

Kunz, J.B., Schwarz, H., and Mayer, A. (2004). Determination of four sequential stages during microautophagy in vitro. The Journal of biological chemistry *279*, 9987-9996.

Li, W.W., Li, J., and Bao, J.K. (2012). Microautophagy: lesser-known self-eating. Cell Mol Life Sci *69*, 1125-1136.

Lin, S.Y., Li, T.Y., Liu, Q., Zhang, C., Li, X., Chen, Y., Zhang, S.M., Lian, G., Liu, Q., Ruan, K., *et al.* (2012). GSK3-TIP60-ULK1 signaling pathway links growth factor deprivation to autophagy. Science *336*, 477-481.

Metzger, S., Saukko, M., Van Che, H., Tong, L., Puder, Y., Riess, O., and

Nguyen, H.P. (2010). Age at onset in Huntington's disease is modified by the autophagy pathway: implication of the V471A polymorphism in Atg7. Hum Genet *128*, 453-459.

Mizushima, N., Yamamoto, A., Hatano, M., Kobayashi, Y., Kabeya, Y., Suzuki, K., Tokuhisa, T., Ohsumi, Y., and Yoshimori, T. (2001). Dissection of autophagosome formation using Apg5-deficient mouse embryonic stem cells. J Cell Biol *152*, 657-668.

Nakagawa, I., Amano, A., Mizushima, N., Yamamoto, A., Yamaguchi, H., Kamimoto, T., Nara, A., Funao, J., Nakata, M., Tsuda, K., *et al.* (2004). Autophagy defends cells against invading group A Streptococcus. Science *306*, 1037-1040.

Nakatogawa, H. (2013). Two ubiquitin-like conjugation systems that mediate membrane formation during autophagy. Essays Biochem *55*, 39-50.

Nazio, F., Strappazzon, F., Antonioli, M., Bielli, P., Cianfanelli, V., Bordi, M., Gretzmeier, C., Dengjel, J., Piacentini, M., Fimia, G.M., *et al.* (2013). mTOR inhibits autophagy by controlling ULK1 ubiquitylation, self-association and function through AMBRA1 and TRAF6. Nature cell biology *15*, 406-416.

Noda, N.N., Satoo, K., Fujioka, Y., Kumeta, H., Ogura, K., Nakatogawa, H., Ohsumi, Y., and Inagaki, F. (2011). Structural basis of Atg8 activation by a homodimeric E1, Atg7. Molecular cell *44*, 462-475.

Ohsumi, Y. (2014). Historical landmarks of autophagy research. Cell research

24, 9-23.

Randow, F., and Munz, C. (2012). Autophagy in the regulation of pathogen replication and adaptive immunity. Trends Immunol *33*, 475-487.

Saitoh, T., Fujita, N., Jang, M.H., Uematsu, S., Yang, B.G., Satoh, T., Omori, H., Noda, T., Yamamoto, N., Komatsu, M., *et al.* (2008). Loss of the autophagy protein Atg16L1 enhances endotoxin-induced IL-1beta production. Nature *456*, 264-268.

Shi, C.S., and Kehrl, J.H. (2010). Traf6 and A20 differentially regulate TLR4-induced autophagy by affecting the ubiquitination of Beclin 1. Autophagy *6*, 986-987.

Taherbhoy, A.M., Tait, S.W., Kaiser, S.E., Williams, A.H., Deng, A., Nourse, A., Hammel, M., Kurinov, I., Rock, C.O., Green, D.R., *et al.* (2011). Atg8 transfer from Atg7 to Atg3: a distinctive E1-E2 architecture and mechanism in the autophagy pathway. Molecular cell *44*, 451-461.

Thompson, A.R., Doelling, J.H., Suttangkakul, A., and Vierstra, R.D. (2005). Autophagic nutrient recycling in Arabidopsis directed by the ATG8 and ATG12 conjugation pathways. Plant Physiol *138*, 2097-2110.

Wang, C., Weerapana, E., Blewett, M.M., and Cravatt, B.F. (2014). A chemoproteomic platform to quantitatively map targets of lipid-derived electrophiles. Nat Methods *11*, 79-85.

Weidberg, H., Shvets, E., Shpilka, T., Shimron, F., Shinder, V., and Elazar, Z.

(2010). LC3 and GATE-16/GABARAP subfamilies are both essential yet act differently in autophagosome biogenesis. EMBO J *29*, 1792-1802.

Yamaguchi, M., Matoba, K., Sawada, R., Fujioka, Y., Nakatogawa, H., Yamamoto, H., Kobashigawa, Y., Hoshida, H., Akada, R., Ohsumi, Y., *et al.* (2012a). Noncanonical recognition and UBL loading of distinct E2s by autophagy-essential Atg7. Nat Struct Mol Biol *19*, 1250-1256.

Yamaguchi, M., Noda, N.N., Yamamoto, H., Shima, T., Kumeta, H., Kobashigawa, Y., Akada, R., Ohsumi, Y., and Inagaki, F. (2012b). Structural insights into Atg10-mediated formation of the autophagy-essential Atg12-Atg5 conjugate. Structure *20*, 1244-1254.

Yamamoto, A., and Simonsen, A. (2011). The elimination of accumulated and aggregated proteins: a role for aggrephagy in neurodegeneration. Neurobiol Dis *43*, 17-28.

Yang, J.J., Lee, Y.J., Hung, H.H., Tseng, W.P., Tu, C.C., Lee, H., and Wu, W.J. (2010). ZAK inhibits human lung cancer cell growth via ERK and JNK activation in an AP-1-dependent manner. Cancer Sci *101*, 1374-1381.

Yi, C., Ma, M., Ran, L., Zheng, J., Tong, J., Zhu, J., Ma, C., Sun, Y., Zhang, S., Feng, W., *et al.* (2012). Function and molecular mechanism of acetylation in autophagy regulation. Science *336*, 474-477.

Youle, R.J., and Narendra, D.P. (2011). Mechanisms of mitophagy. Nature reviews Molecular cell biology *12*, 9-14.

Zalckvar, E., Berissi, H., Mizrachy, L., Idelchuk, Y., Koren, I., Eisenstein, M., Sabanay, H., Pinkas-Kramarski, R., and Kimchi, A. (2009). DAP-kinase-mediated phosphorylation on the BH3 domain of beclin 1 promotes dissociation of beclin 1 from Bcl-XL and induction of autophagy. EMBO reports *10*, 285-292.

Zhao, J., Brault, J.J., Schild, A., Cao, P., Sandri, M., Schiaffino, S., Lecker, S.H., and Goldberg, A.L. (2007). FoxO3 coordinately activates protein degradation by the autophagic/lysosomal and proteasomal pathways in atrophying muscle cells. Cell metabolism *6*, 472-483.

국문 초록

세포자가섭식 작용 (영문: Autopahgy)은 세포질 내의 가수 분해 효소를 함유한 기관중의 하나인 리소좀을 통해 자가포식 소체 형성과정에 관여하는 이화과정이다. 세포는 여러 자가섭식 관련 단백질 (ATGs) 을 이용하여 이중막 구조의 소포 구조를 가지는 자가포식 소체 (autophagosome)를 생성하며, 자가포식 소체는 리소좀과 결합함으로서 미토콘드리아 및 단백질 응집체 또는 노화, 손상을 입은 세포질 내 구성요소를 제거한다. 세포자가섭식 작용은 세포 사멸 및 병인 제거, 종양생성, 신경변성질환 및 노화를 포함한 세포내 항상성을 유지하는데 역할을 하기때문에 그 분자적 기작을 이해 하는 것은 매우 중요하다. 현재까지 여러 자가섭식 관련 유전자 (ATGs) 와 분자기작을 포함하는 그들의 기능이 밝혀져 왔지만, 자가포식 소체의 개시 및 신장의 정확한 조절 기작과 그 기능은 여전히 알려지지 않았다. 따라서 세포자가섭식 과정의 새로운 조절자를 찾고 그 기작을 명확하게 하기 위해 저자는 동물 세포에 기초한 이분자간의 상호 결합에 의해 형광을 발생시키는 (Bimolecular fluorescence complementation; 약어

BiFC) 스크리닝 방법을 도입하였다.

저자는 세포자가섭식 과정을 매개하는 유전자들인 ULK1과 ATG9 단백질간의 상호 결합을 확인하고 ULK1을 조절하는 상위 단계의 조절자를 찾기위해 둘 간의 상호 결합을 이용하였다. 두 유전자를 BiFC 분석 방법에 사용하였으며 이는 각각 BiFC의 아미노 말단에 부착된 ULK1 과 카르복시 말단에 부착된 ATG9 간의 결합에 의하여 세포내에서 형광을 발하게 된다. 이를 동물 세포주를 이용하여 cDNA library 스크리닝 에 적용하였으며 cDNA library 유전자를 과발현 시켜 그 기능을 회복 시켜주는 스크리닝 방법을 응용하여 BiFC를 통해 세포자가섭식 과정을 활성화 시켜주는 유전자로서 G6PT를 동정 하였다. G6PT는 수송활성을 담당하는 단백질로서 ULK1과 ATG9 간의 상호 결합을 강화 시켜 BiFC의 형광 활성을 증가 시켰으며 기존에 알려진 G6PT의 수송활성능력과 별개로 자가섭식을 조절하는 기능을 가지는 것을 확인하였다. 기작연구에 있어 mTORC1 단백질은 자가섭식과정을 억제하는 역할을 한다. G6PT는 이러한 mTORC1 단백질의 활성을 억제함으로서, 결과적으로 자가섭식 과정을 활성화 시키며 따라서 mTORC1의 상위 단계에서 이를

조절함으로 자가섭식 과정을 조절한다.

세포는 번역 후 수정(PTM) 에 의해 환경적인 스트레스에 재빠르게 적응한다. 다양한 종류의 PTM 중 인산화에 의해 자가섭식의 신장단계를 조절 할 수 있는 유전자를 동정해내기 위하여 두 자가섭식 관련 유전자를 사용하는 스크리닝 방법을 도입하였다. ATG7은 자가섭식 과정중 E1의 기능을 하며 ATG12는 그 기질로서 자가섭식의 신장과정에서 중요한 기능을 하는 것으로 보고되어 있다. 따라서 새로운 단백질을 동정하기 위하여 BiFC 를 도입하여 아미노 말단에 부착된 ATG7 과 카르복시 말단에 부착된 ATG12 을 제작하였다. 인산화와 탈 인산화를 관장하는 유전자의 cDNA library를 동물세포에서 스크리닝 함으로서 잠재적인 자가섭식 과정의 활성자인 ZAK을 동정하였다. ZAK 단백질을 과발현 시켰을 경우 자가섭식의 활성이 증가 하였으며 반대로 세포내에서 ZAK 의 발현을 줄여주었을 경우 영양분의 결핍에 의한 자가섭식이 현저하게 감소하는 것을 관찰하였다. 따라서 ZAK이 ATG7과의 결합과 그 인산화 활성을 통해 자가섭식 과정을 조절하는 것으로 가정 할 수 있다.

주요어: 자가섭식 개시 및 신장, ATGs, G6PT, BiFC, mTORC1, ZAK

학번: 2010-30923